Genetic analysis of *Mycobacterium abscessus* reveals genomic diversity linked to global plasmid distribution

Kensuke Ohse[1], Atsushi Yoshida[2,3,4], Keisuke Kamada[3,5], Hironobu Kitazawa[6,7], Yusuke Ito[8], Takayo Shoji[9], Kenichiro Watanabe[10], Hiroshi Koganemaru[2], Ken Kikuchi[3] and Masashi Toyoda[1,11,*]

[1]Research Team for aging science (Vascular Medicine), Tokyo Metropolitan Institute for Geriatrics and Gerontology (TMIG), Tokyo, Japan

[2]Department of Infectious Diseases, TMIG, Tokyo, Japan

[3]Department of Infectious Diseases, Tokyo Women's Medical University, Tokyo, Japan

[4]Department of Genetic Diagnosis and Laboratory Medicine, Dokkyo Medical University, Tochigi, Japan

[5]Department of Mycobacterium Reference and Research, The Research Institute of Tuberculosis, Japan Anti-Tuberculosis Association, Tokyo, Japan

[6]Department of Pediatrics, Nagoya University Graduate School of Medicine, Aichi, Japan

[7]Department of Hematology and Oncology, Children's Medical Center, Japanese Red Cross Aichi Medical Center Nagoya First Hospital, Aichi, Japan

[8]Department of Pediatric Infectious Diseases, Hyogo Prefectural Amagasaki General Medical Center, Hyogo, Japan

[9]Department of Infectious Diseases, Shizuoka Children's Hospital, Shizuoka, Japan

[10]Department of Hematology and Oncology, Shizuoka Children's Hospital, Shizuoka, Japan

[11]Lead contact

*Correspondence:mtoyoda@tmig.or.jp

SUMMARY

Genetic epidemiological analysis of mobile genetic elements, such as plasmids, has rarely been carried out in *Mycobacterium abscessus,* regardless of its usefulness in speculating the past contact between bacteria. In this study, through whole genome sequencing analysis of clinical isolates of *M. abscessus* sequentially collected from the same patient, we identified a single nucleotide variant that could cause antibiotic resistance, and three plasmids (pMAB625-1, pMAB625-2 and pMAB625-3) not found in the type strain. We investigated the distribution of plasmids previously identified in *M. abscessus,* including pMAB625 plasmids, in 462 clinical isolates worldwide *in silico*. pMAB625-3 was detected in the largest number of isolates. Furthermore, phylogenetic tree analysis revealed that these plasmids transferred beyond regions and subspecies and acquired unique mutations. These results indicate that transmission of plasmids increases the genomic diversity in *M. abscessus,* and plasmid epidemiology is useful for estimating the past contact between bacteria.

KEYWORDS

Mycobacterium abscessus; Whole genome sequencing; Plasmid; Horizontal gene transfer

INTRODUCTION

In recent years, the threat of antimicrobial-resistant bacteria has been increasing worldwide, and they could be responsible for 1.91 million deaths per year by 2050[1]. Hence, research into the mechanisms and routes of transmission is becoming increasingly important to develop effective countermeasures against antimicrobial-resistant bacteria. The global incidence of non-tuberculous mycobacterial infections has been on the rise, presenting a significant challenge due to their increasing prevalence and innate drug resistance, particularly in *Mycobacterium abscessus* infections[2]. *M. abscessus* is not limited to pulmonary infections but also serves as the causative agent for various extrapulmonary infections, including bloodstream, skin, soft tissue, surgical site, and peritoneal dialysis-related infections[3]. Furthermore, it demonstrates resistance to a wide range of antimicrobial agents.

The route of infection of *M. abscessus* remains controversial. It has been assumed that *M. abscessus* is transmitted from the environment, such as soil and water systems, and person-to-person transmission does not occur. However, a few cases of suspected person-to-person transmission have been reported[4–6]. In addition, the existence of "dominant clones", which were isolated in almost all regions and phylogenetically close[6,7], makes the source and transmission routes of the bacteria mysterious[8].

Whole genome sequencing (WGS) analysis and phylogenetic tree analysis of the core genome, which is the genomic region shared by all isolates, are often conducted to predict the origin and transmission route of the isolates[9]. However, the accessory genome, which is shared by a certain percentage but not all of the isolates such as plasmids, prophage, and genomic islands, is made up of approximately 30% of the typical number of all genes of *M. abscessus*[10]. Therefore, the analysis of the pan-genome, which includes both the core genome and accessory genome, was performed to compare the genetic relation of all gene sets of *M. abscessus*[8,11]. Although the pan-genome analysis has the advantage of comparing whole bacterial genomes, it has the disadvantage of analyzing accessory genomes as gene units, resulting in the loss of information on the units of mobile genetic elements. Therefore, epidemiological analysis of mobile genetic element units, such as individual plasmids, may more accurately predict the origin and route of infection of bacteria.

In this study, we performed the WGS analysis of the clinical isolates that acquired elevated minimum inhibitory concentrations (MICs) for carbapenem antibiotics in a case of disseminated infection caused by *M. abscessus* subsp. *abscessus* (ABS) during antimicrobial therapy. We detected one mutation potentially responsible for antimicrobial resistance (AMR) and identified three plasmids (pMAB625-1, pMAB625-2 and pMAB625-3) that type strain did not harbor. Therefore, we analyzed the distribution of plasmids identified in *M. abscessus* before, including pMAB625 plasmids and found that pMAB625-3 was the most widely spreading plasmid among the clinical isolates of *M. abscessus* worldwide. Thus, we investigated whether predicting the past contact between isolates is possible by analyzing single nucleotide variants (SNVs) and structural variants (SVs) of the plasmids.

RESULTS

The clinical isolates had decreased susceptibility to carbapenem antibiotics compared to the type strain

We sequentially isolated five ABS strains from one patient who had osteomyelitis over six months (Table 1). We first compared the growth rate and antimicrobial susceptibility of these clinical isolates with the type strain (ATCC 19977). The growth rates of Isolate57625 and Isolate57626 were significantly slower than the type strain (Figure S1). Antimicrobial susceptibility testing showed that the MIC of Isolate57626 against IPM, which binds the penicillin-binding proteins (PBPs) and inhibits the bacterial cell wall synthesis, was higher than that of the type strain (Table 1). The MICs of Isolate57625 and Isolate57626 against meropenem (MEPM), which has the same mechanism of action as IPM and improved stability, were higher than that of the type strain (Table 1). However, there were no differences in MIC between ATCC 19977 and two isolates against the other antibiotics. These results indicated the decreased susceptibility of the isolates to carbapenem antibiotics compared to the type strain.

87

88 ***WGS of the clinical isolates***

89 To explore the factors determining the difference in growth rate and antimicrobial susceptibility between the
90 type strain and the clinical isolates, we performed WGS using short-read sequencer and Nanopore long-
91 read sequencer. We analyzed the *de novo* assembled chromosome sequences and found that two large
92 insertions (13 kbp and 8 kbp) and a deletion (16 kbp) existed in the sequence of Isolate57625 (Figure S2A,
93 B). The coding sequences of phage integrase and transposase were present near the three large SVs
94 (Figure S3), indicating that these regions were prophage and transposon. We also analyzed the SNVs in
95 the chromosome (Table S3), however, we could not identify the cause of the phenotypic differences.
96 Phylogenetic analysis showed that the isolates were genetically close to the type strain (Figure S2C).
97 Furthermore, to analyze the difference in the chromosome sequence between five clinical isolates, we
98 analyzed SVs and SNVs between the isolates (Figure S4). This analysis suggested one mutation located
99 at the putative *PbpA*, which was associated with the synthesis of the bacterial cell wall[12] and the target of
100 carbapenem antibiotics[13], may be responsible for the reduced susceptibility of Isolate57626 to IPM
101 compared to Isolate57625.

102

103 ***The isolates had three plasmids that encode various virulence factors***

104 WGS analysis also revealed that the clinical isolates have three plasmids not found in the type strain
105 (named pMAB625-1, pMAB625-2 and pMAB625-3, respectively) (Table 2). Thus, we next focused on the
106 pMAB625 plasmids and compared the pMAB625 plasmid sequences with other plasmids registered to
107 PLSDB[14] previously (Table 3). A taxonomic keyword search for "*abscessus*" returned 20 plasmids. To
108 investigate the homology between these plasmids, we calculated ANI between them and pMAB625. No
109 plasmid had a high ANI for pMAB625-1, however, the ANI between pMAB625-2 and pGD21-2 was 97.4%
110 with some SVs. Furthermore, the ANI for pMAB625-3 against pGD69A-1 and pGD42-1 was 100%. These
111 results indicated that pMAB625-2 and pMAB625-3 were retained in the other clinical isolates of *M.*
112 *abscessus.* Next, we performed qPCR using primers specific to each plasmid to verify the copy numbers
113 of pMAB625 plasmids in the clinical isolates. This analysis showed that the copy number of pMAB625-1
114 and pMAB625-2 was less than one per bacterium, and that of pMAB625-3 was more than five per bacterium
115 in the isolates (Figure S5). Therefore, the clinical isolates were considered to be a heterogeneous
116 population in terms of plasmid possession.

117

118 We then investigated the function of the genes encoded on pMAB625 plasmids using homology search.
119 Plasmids encode various factors that influence host characteristics. Therefore, we listed the lost and
120 acquired genes in Isolate57625 compared to the type strain to investigate the factors affecting antimicrobial
121 susceptibility (Table S4). Of note, 480 candidate open reading frames (ORFs) were acquired and 37
122 candidate ORFs were lost in Isolate57625 compared to the type strain. We then searched the AMR genes
123 from several databases using Blast+ based on the amino acid sequences of the acquired candidate ORFs.
124 This analysis showed that the coding sequence (CDS) named Isolate57625_54550 had a similarity to *qacA*,
125 a subunit of the qac multidrug efflux pump[15], (identity, 31 %; *e*-value, 1.69e-10; coverage, 16.1%) and that
126 the CDS named Isolate57625_54800 had a similarity to *MexL*, a specific repressor of *MexJK* multidrug
127 efflux system[16] (identity, 33%; *e*-value, 5.54e-4; coverage, 34.4%). However, the identity and coverage
128 were not sufficiently high.

129

130 To gain further insight into the effect of gene acquisition, we searched the homology of the acquired
131 candidate ORFs using the mycobacterial gene database of Mycobrowser[17]. This analysis detected 37
132 mycobacterial proteins with amino acid homology to candidate ORFs of the isolates (identity > 30 %, *e*-
133 value < 1e-50) (Table S5). Notably, genes associated with the ESX secretion system were highly enriched

134 (10/37, 27%). ESX secretion systems are encoded in various bacteria on their chromosomes and plasmids.
135 It has been reported that the ESX secretion system (also known as the type VII secretion system) is involved
136 in bacterial virulence through several mechanisms, including evasion of the host immune system[18,19], and
137 biofilm formation[20]. We further searched whether other ORFs of the components of the ESX secretion
138 system were encoded near the loci of the detected ORFs of the components of the ESX secretion system
139 using blast+. We detected several components of the ESX secretion system in pMAB625-1 and pMAB625-
140 2 (Figure 1A). Core genes that construct membrane pores (*eccB, eccC, eccD, mycP,* and *eccE*) were
141 present in these gene clusters. The type strain and clinical isolates have ESX-3 and ESX-4 loci on their
142 chromosomes; therefore, the isolates acquired two additional ESX loci by the plasmid acquisition. To predict
143 the function of these genes, we performed phylogenetic tree analysis using known amino acid sequences
144 of the ESX secretion system components in chromosomes and plasmids. It was previously reported that
145 plasmid-encoded ESX loci can be classified into 4 major clusters[21]. Importantly, our analysis revealed that
146 plasmid-encoded ESX loci were classified into 5 major clusters (ESX-P cluster 1-5) (Figure 1B). Notably,
147 the newly classified ESX-P cluster 5 contained the ESX loci of pMAB625-1 and pMAB625-2. As shown in
148 the results of the plasmid homology search (Table 3), the ESX loci of pGD21-2 and pMAB625-2 were
149 genetically close. The ESX loci of pMAB625-1 were genetically close to that of pMFLV01, which was
150 harboured by *Mycobacterium gilvum* PYR GCK. It was previously reported that pMFLV01 was enriched in
151 biofilm formed in household water purifiers by metagenomic analysis[22]. Biofilm formation is one of the drug
152 resistance mechanisms in mycobacterium and acts as a barrier against antibiotics. We also detected the
153 toxin-antitoxin (TA) system components, YefM/YoeB and VapB5/VapC5 in pMAB625-1. The TA system is
154 present in various bacteria and archaea and encoded on their chromosomes and plasmids. It contributes
155 to plasmid persistence, inhibiting bacteriophage propagation, and increases antimicrobial tolerance by
156 inducing dormancy[23]. These results indicated that the clinical isolates acquired factors that could contribute
157 to bacterial virulence through plasmid transfer.

158

159 ***Gene expression analysis on the pMAB625 plasmids in the clinical isolates***

160 We found that the various genes associated with bacterial virulence were encoded on the pMAB625
161 plasmid. However, it was unclear whether genes encoded on these plasmids were expressed in the isolates
162 and to what extent gene expression on the plasmids influenced the expression of genes on the
163 chromosome. To address this question, we analyzed the global gene expression in the type strain and the
164 isolates using RNA-seq analysis (Figure 1C and Table S6). The expression levels of the genes on plasmids
165 were low to moderate (below the 75th percentile of the distribution of expression levels of all genes that
166 were expressed in the isolates and the type strain). Notably, the expression levels of the most genes (19/27
167 genes) associated with the ESX secretion system, which were encoded on the pMAB625-1 and pMAB625-
168 2, were moderate (below the 75th percentile and above the 25th percentile) (Figure 1C). In addition, the
169 genes associated with the TA system and the mycobacterial membrane protein large (MMPL) family
170 transporter, which were also encoded on the pMAB625-1 and pMAB625-3, respectively, were expressed
171 at moderate levels. These results indicated that the numerous genes associated with bacterial virulence
172 encoded on the plasmids were expressed at moderate levels in the clinical isolates, despite the low number
173 of copies per bacterium for the pMAB625-1 and pMAB625-2. Next, in the clinical isolates, 393 genes were
174 highly expressed and 29 genes were low expressed compared to the type strain. Of these differentially
175 expressed genes, 87.2% of genes (368 highly expressed genes) were acquired genes by SVs or plasmids,
176 and 12.8% of the genes (25 highly expressed genes and 29 low expressed genes) were present on the
177 chromosomes of both the isolates and the type strain (Figure 1C). These results indicated that the gene
178 expression on the plasmid could directly or indirectly affect the expression on the chromosome but to a
179 lesser extent.

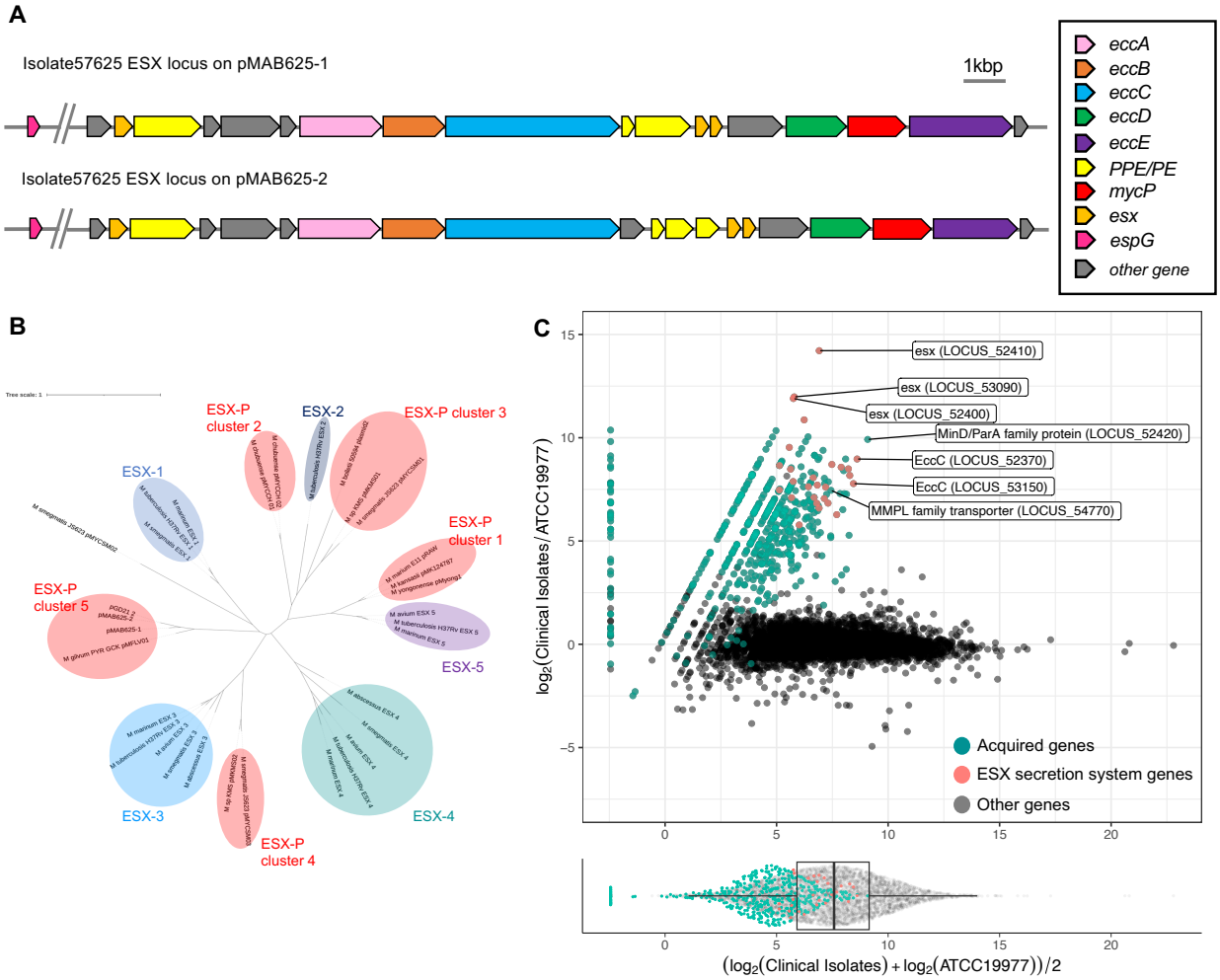

Figure 1. Phylogenetic and gene expression analysis of the genes related to the ESX secretion system

(A) The loci of the ESX secretion system are encoded on pMAB625-1 and pMAB625-2. CDSs of the ESX secretion system were searched using Blast+. The core components that construct membrane pore (*eccB, eccC, eccD, mycP,* and *eccE*) are contained in this operon.

(B) Phylogenetic tree analysis of various ESX loci encoded on chromosomes and plasmids. The amino acid sequence of the genes that construct the membrane pore were concatenated and the phylogenetic tree was created by NGphylogeny.fr[24] using the PhyML+SMS inference method. The classification of each cluster was followed as previously reported[21].

(C) RNA-seq analysis of the type strain and the isolates. The x-axis represents the mean log expression levels, and the y-axis of the top plot represents the log fold change. The bottom dot plot and box plot represent the distribution of the expression levels of each gene. The green dots represent the data of genes that the isolates acquired by SVs and plasmid acquisition. The red dots represent the data of ESX secretion system genes encoded on the plasmids.

pMAB625 plasmids were globally distributed in the clinical isolates of M. abscessus

So far, we have found that the isolates carried three plasmids that the type strain did not, that these plasmids encoded the genes that could contribute to bacterial virulence, and that these genes also expressed in the

isolates. However, we had analyzed the strains sequentially isolated from only one patient and it was uncertain whether the plasmid acquisition occurred extensively in clinical isolates of mycobacterium. We therefore investigated whether other clinical isolates of mycobacterium carry the pMAB625 plasmids. We first performed PCR using the genomic DNA of the clinical isolates collected in Japan[25] with primers specific to each pMAB625 plasmid. We detected pMAB625-3 in two isolates other than Isolate57625, although we did not detect pMAB625-1 and pMAB625-2 in any isolates other than Isolate57625 (Figure 2A). Both the isolates in which pMAB625-3 was detected were *M. abscessus*. We then verified the plasmid possession by mapping the read data from the short-read sequencer to the pMAB625 plasmid sequences. We used the read data of *M. abscessus* clinical isolates in Japan[7] obtained from the NCBI database in addition to our original data. Out of 125 clinical isolates, pMAB625-2 was detected in four isolates (3.2%) and pMAB625-3 was detected in 16 isolates (12.8%) (Figure 2B). These isolates were collected from the four prefectures in Japan (Tokyo, Shizuoka, Aomori, and Okinawa) (Figure 2C). We also mapped the read data of the other mycobacterium species (three of *Mycobacterium iranicum*, 20 of *Mycobacterium fortuitum*, and 25 of *Mycobacterium chelonae*), however, no pMAB625 plasmid was detected in these isolates (data not shown).

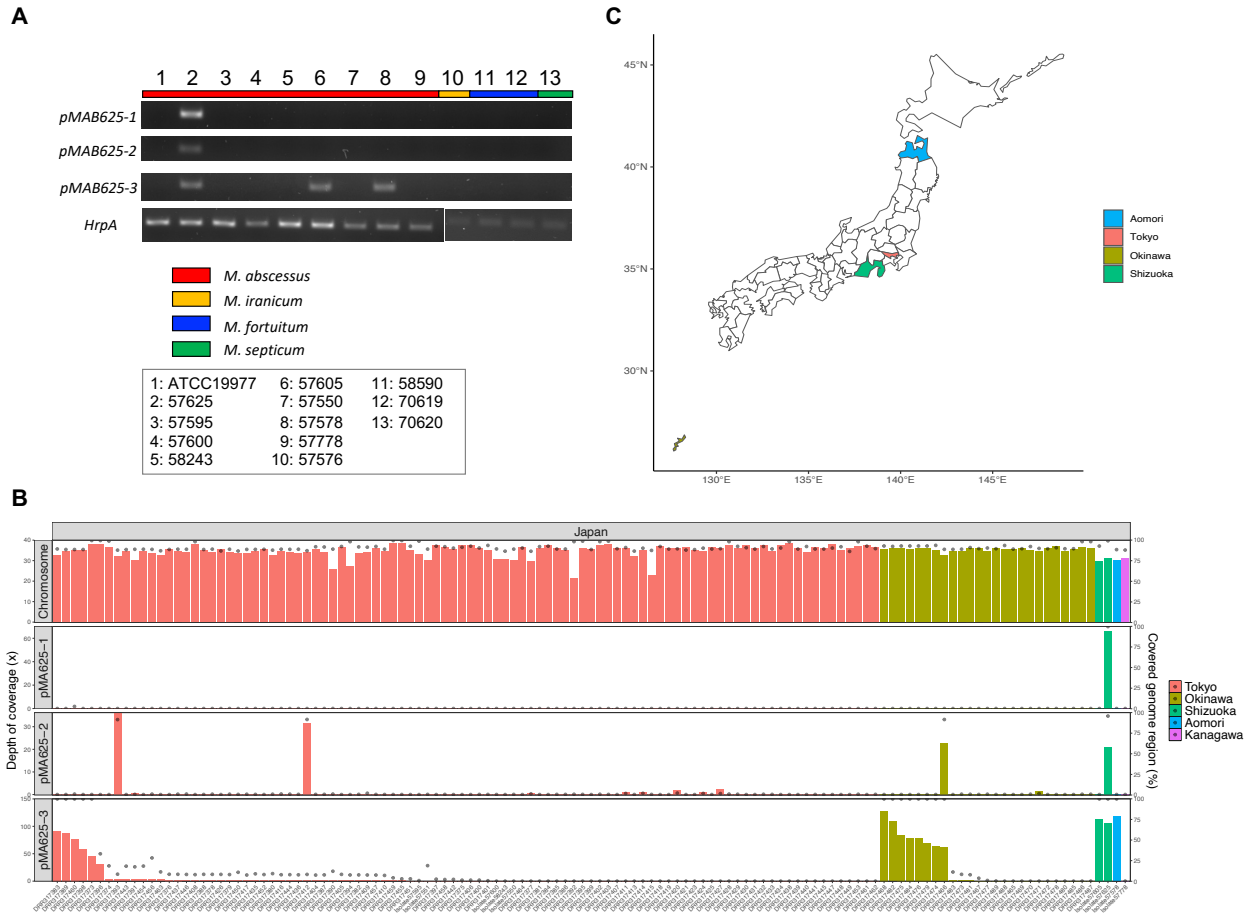

Figure 2. The distribution of pMAB625 plasmid in the clinical isolates in Japan

(A) PCR analysis of the possession of pMAB625 plasmid in the clinical isolates which our group isolated in Japan. PCR was performed using the primers specific to each plasmid and *HrpA*. The color bar represents the species of each isolate. The primer sets of *HrpA* were different depending on the species.

(B) Mapping the read data of the clinical isolates in Japan to Isolate57625 genome sequence. The bar plot represents the depth of coverage to chromosome and each plasmid and the dot plot represents the percentage of covered genome region.
(C) Geographical map of Japan. The prefectures in which the pMAB625 plasmids were detected are represented by color.

Moreover, to investigate whether clinical isolates in other areas of East Asia possess pMAB625 plasmids, we mapped the available read data about the clinical isolates from Taiwan[7] and China[26]. pMAB625-2 was detected in the isolates from China (2/69, 2.9%) and pMAB625-3 was detected in the isolates from Taiwan (8/98, 8.2%), and China (5/69, 7.2%) (Figure S6). Two plasmids were detected in ABS and *M. abscessus* subsp. *massiliense* (MAS) but not in *M. abscessus* subsp. *bolletii* (BOL). In addition, we analyzed the clinical isolates in Spain, the UK, and the US to determine whether these isolates carried the pMAB625 plasmids (Table 4). pMAB625-2 plasmid was detected in isolates from the UK (2/30, 6.7%), and the US (2/110, 1.8%). pMAB625-3 plasmid was detected in the isolates from Spain (9/30, 30%), the UK (1/30, 3.3%), and the US (14/110, 12.7%). Overall, pMAB625-1 was detected in one isolate (1/462, 0.2%), pMAB625-2 was detected in 10 isolates (10/462, 2.2%), and pMAB625-3 was detected in 53 isolates (53/462, 11.5%).

As previous analyses have shown that the pMAB625 plasmids are retained in many clinical isolates, we investigated to what extent other plasmids are retained in the clinical isolates. First, we searched the plasmid sequence in PLSDB as the taxonomic name for "*abscessus"* and got 20 plasmid sequences (Table 3). We removed three plasmids (pGD42-1, pGD69A-1 and FDAARGOS_1640_plasmid) because they were identical to other plasmids with no SV. We selected 20 plasmids shown in Table 3 as "TRUE" for "USE for Reference" together with three pMAB625 plasmids. Then, we mapped the read data of the clinical isolates to these plasmid sequences. Except for the pMAB625 plasmid, three plasmids (pGD69A-2, pGD22-2, and pGD42-2) were detected in more than 10 isolates (Table 4). Seven plasmids (pGD21-1, pGD21-2, pGD22-1, pGD25-3, pJCM30620_2, BRA100 and 50594_plasmid1) were not detected in our dataset. Statistical analysis showed regional differences in the frequency of appearance of these plasmids (Table 4). pGD69A-2 was detected more frequently in the US (9/110, 8.2%) than in Japan (0/125, p=0.014). pGD22-2 was detected more frequently in Spain (3/40, 13.3%) than in Japan (0/125, p=0.018) and Taiwan (0/98, p=0.036). pGD42-2 was detected more frequently in Spain (4/30, 13.3%) than in Japan (0/125, p=0.017). pGD42-2 was also detected more frequently in the US (12/110, 10.9%) than in Japan (0/125, p=0.001), China (0/69, p=0.045), and Taiwan (1/98, 1.0%, p=0.041). pGD25-1 was detected more frequently in the UK (4/30, 13.3%) than in Japan (0/125, p=0.018) and in Taiwan (0/98, p=0.036). Moreover, we performed a phylogenetic tree analysis of the chromosomes to determine whether these plasmids are horizontally transferred or whether the same strains harboring the plasmids are spreading (Figure 3). The phylogenetic tree analysis showed that pGD22-2 and pGD42-2 were only detected in the isolates belonging to Clade756. In contrast, pMAB625-3 was detected mainly in the isolates belonging to the four clades (Clade595, 674, 791 and 813). pGD25-1 and pGD69A-2 were detected mainly in the isolates belonging to Clade678 and Clade813. pMAB625-2 and pGD19 were also detected in the isolates belonging to several clades. These results indicated that some plasmids, such as pMAB625-3, were spread across clades and others were restricted to the specific clade.

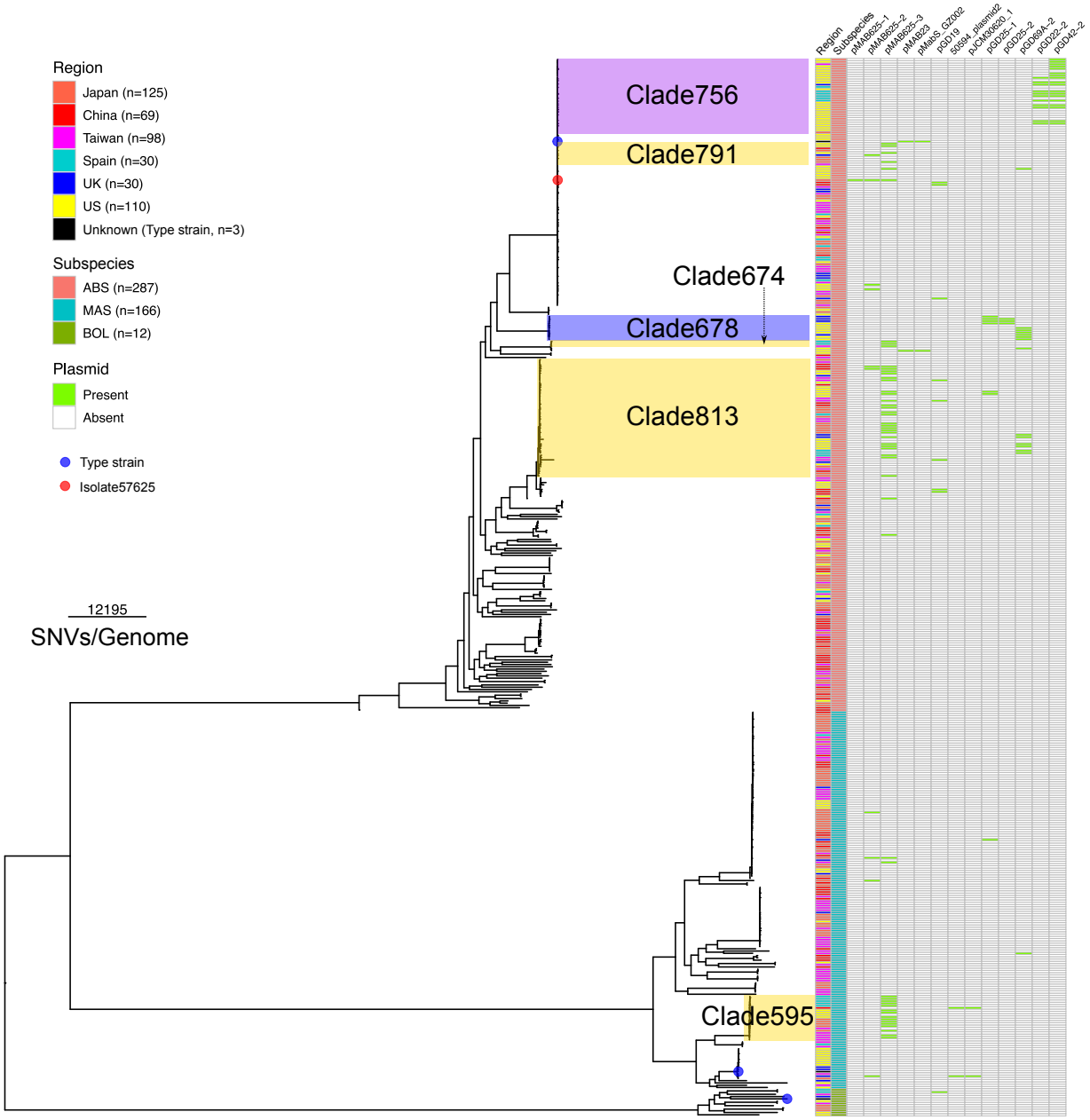

Figure 3. The relation between the phylogenetic distance of host bacterial chromosomes and plasmid distribution in clinical isolates worldwide

The phylogenetic tree was created by Gubbins[27] using chromosome sequences and visualized by ggtree[28]. The read data of the clinical isolates collected worldwide were mapped to pMAB625 and known plasmid sequences to verify the plasmid distribution. Tree-scale represents the number of SNVs per genome.

Phylogenetic and structural variant analysis of pMAB625 plasmids enabled the strict classification of isolates and prediction of past inter-subspecies contact

273 So far, we acquired the sequence information for pMAB625-3, which is retained in 53 different clinical
274 isolates, and for pMAB625-2, which is retained in 10 different clinical isolates. Therefore, we examined the
275 genetic relation between the plasmids and investigated whether it could predict host origin and route of
276 transmission. At first, we performed a phylogenetic tree analysis of 53 sequences of pMAB625-3 (Figure
277 4A). Forty-two sequences (covered by a yellow box in Figure 4A) belonged to the same clade of the
278 sequence of pMAB625-3 in Isolate57625. However, 11 sequences belonged to the different clades. In
279 particular, the pMAB625-3 sequence of SRR7800511 (US, Clade595) was genetically distant from other
280 pMAB625-3 sequences in the isolates belonging to Clace595. The pMAB625-3 sequence of DRR317373
281 (Japan, Clade791) was also genetically distant from other pMAB625-3 sequences in the isolates belonging
282 to Clade791. These results suggested that plasmid epidemiology, when combined with core-genome
283 analysis, could accurately predict the classification of clinical isolates. In addition, the verification of the
284 mapping results also showed that pMAB625-3 sequences in the six isolates (DRR317373, Japan;
285 SRR18969469, China; SRR7800518, US; SRR7800703, US; SRR7800409, US; SRR7800511, US) were
286 heterogeneous because the unmutated reads and mutated ones were mixed (Figure 4B). Thus, we ran
287 freebays with the parameter "--ploidy 2" to detect SNVs in these mixed reads. Interestingly, the variant
288 hotspot region was located at the CDS of the MMPL family transporter, which was the most reliably highly
289 expressed gene in Isolate57625 and the other four isolates in the RNA-seq analysis. The variant pattern in
290 the MMPL family transporter was classified into three types (Figure 4B). Four sequences (DRR317373,
291 Japan; SRR7800518, US; SRR7800703, US; SRR7800409 US) were classified as Type A and one
292 sequence each was classified as Type B (SRR18969469, China) and Type C (SRR7800511, US), the other
293 47 sequences had no mutation. There were three missense mutations and 14 or 15 silent mutations in Type
294 A, 20 missense mutations and 43 silent mutations in Type B, and 47 missense mutations and 126 silent
295 mutations in Type C (Table S7). Surprisingly, despite many mutations, no mutation was responsible for the
296 frameshift and nonsense mutations. It was therefore speculated that the mutant MMPL family transporters
297 were being translated into full-length proteins in these isolates. Thus, these data indicated that pMAB625-
298 3 was spread across strains and regions, each acquiring unique mutations and some clinical isolates
299 retaining pMAB625-3 expressed mutated MMPL family transporters.

300

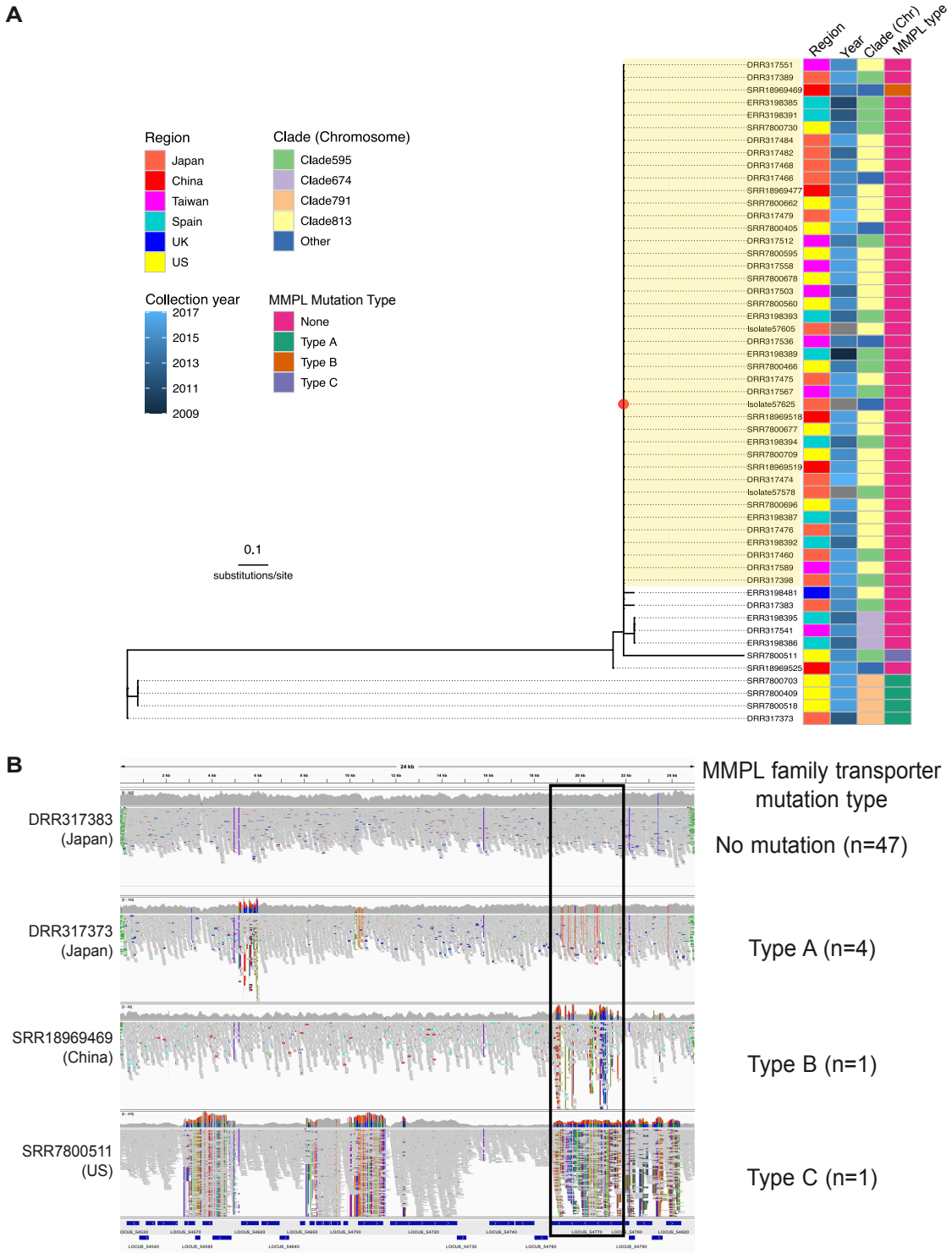

Figure 4 Phylogenetic tree and SNVs analysis of pMAB625-3

(A) Phylogenetic tree of the sequences of pMAB625-3 detected in the 53 isolates. The phylogenetic tree was created using the maximum-likelihood method using iQ-TREE2 based on the core-SNVs data. The sequences belonging to the clade covered by yellow color were identical, although the sequence of SRR18969469 was heterogeneous. The classification of “Clade (Chromosome)” is based on the clade in

307 the phylogenetic tree indicated in Figure 3. pMAB625-3 sequences of the isolates covered by yellow box
308 were identical except for SRR18969469, whose sequence of MMPL family transporter was mixed.

309 (B) The classification of the pMAB625 sequences based on the SNVs. The mapping results of the reads
310 data from each isolate to pMAB625-3 were also visualized by IGV. The mutation hotspot was located at
311 the MMPL family transporter (surrounded by a black line square). The mutation types of the MMPL
312 transporters were classified into three types, and all mutations at this region were missense or silent.

313

314 Then, we classified pMAB625-2 sequences in terms of SVs. The sequences of pMAB625-2 were classified
315 into four types (Figure 5A). Assuming that Type I, which was the sequence of pMAB625-2 in Isolate57625,
316 was the base sequence, Type II and III had the large SVs at Region B, and Type II but not Type III had at
317 Region C. In contrast, Type IV had large SVs at Region A and C but not at Region B. Type I, Type III, and
318 Type IV were detected in ABS, and Type II was detected in MAS, except for ERR3198514. In addition,
319 Type III was detected only in the isolates collected in China, and Type IV was detected only in the isolates
320 collected in the US. All pMAB625-2 sequences retained the ESX locus. These results indicated that
321 pMAB625-2 had been horizontally transferred between subspecies and had acquired the SVs unique to
322 each subspecies and region. Next, we analyzed the relation between the phylogenetic distance of hosts'
323 chromosome sequences and pMAB625-2 type (Figure 5B). The distribution of the pMAB625-2 type was
324 almost consistent with the phylogenetic relation of hosts' chromosomes. However, the pMAB625-2 type of
325 Isolate57625 and ERR3198415 were different from those of the other isolates belonging to the same clade
326 of phylogenetic tree of hosts' chromosomes. Interestingly, Type II was detected in four MAS isolates but
327 also in ERR3198415 whose subspecies was ABS. This result indicated the possibility of direct or indirect
328 contact between ERR3198415 and the other four MAS isolates in the past, especially with ERR3198440
329 isolated from the same region.

330

331 Finally, we investigated the distribution in our dataset regarding the plasmids identified in other NTMs
332 except for *M. abscessus* to verify whether plasmids transferred between *M. abscessus* and other NTM
333 species. Recently, Wetzstein *et al*. reported clinical and genomic features in Europe about *Mycobacterium*
334 *avium* complex (MAC)[29], the most frequently detected NTM globally[30,31]. In the report, they investigated the
335 distribution of the known 152 plasmids registered in PLSDB and showed that plasmids identified in *M.*
336 *abscessus*, including pGD69B-1 (identical to pGD69A-1) and pGD42-1, which were identical to pMAB625-
337 3, were not detected in their dataset. Therefore, we investigated the distribution of these 152 plasmids in
338 our dataset using our methods in this study. As a result, we detected the same plasmids indicated in Table
339 3 but did not other plasmids identified in other NTM except for pMN23 (accession number: NC_010604.1)
340 and pMFLV03 (accession number: NC_009341.1) in two and one isolates, respectively (Table S8). pMN23
341 was almost identical to pMAB23 (ANI: 99.9%), so pMN23 was detected redundantly in ATCC 19977 and
342 SRR7800408, which had pMAB23. Interestingly, pMFLV03 was detected in ERR3198408 (covered
343 genome region: 78.7%, depth of coverage: 73.1x). pMN23 had originally identified in *Mycobacterium*
344 *marinum*[32] and pMFLV03 had identified in *M. gilvum* PYR-GCK (according to the GenBank registry
345 information), indicating that these plasmids could be present across NTM species. These results suggested
346 that plasmid distribution is strictly different from *M. abscessus* and other NTMs except for very few cases.

347

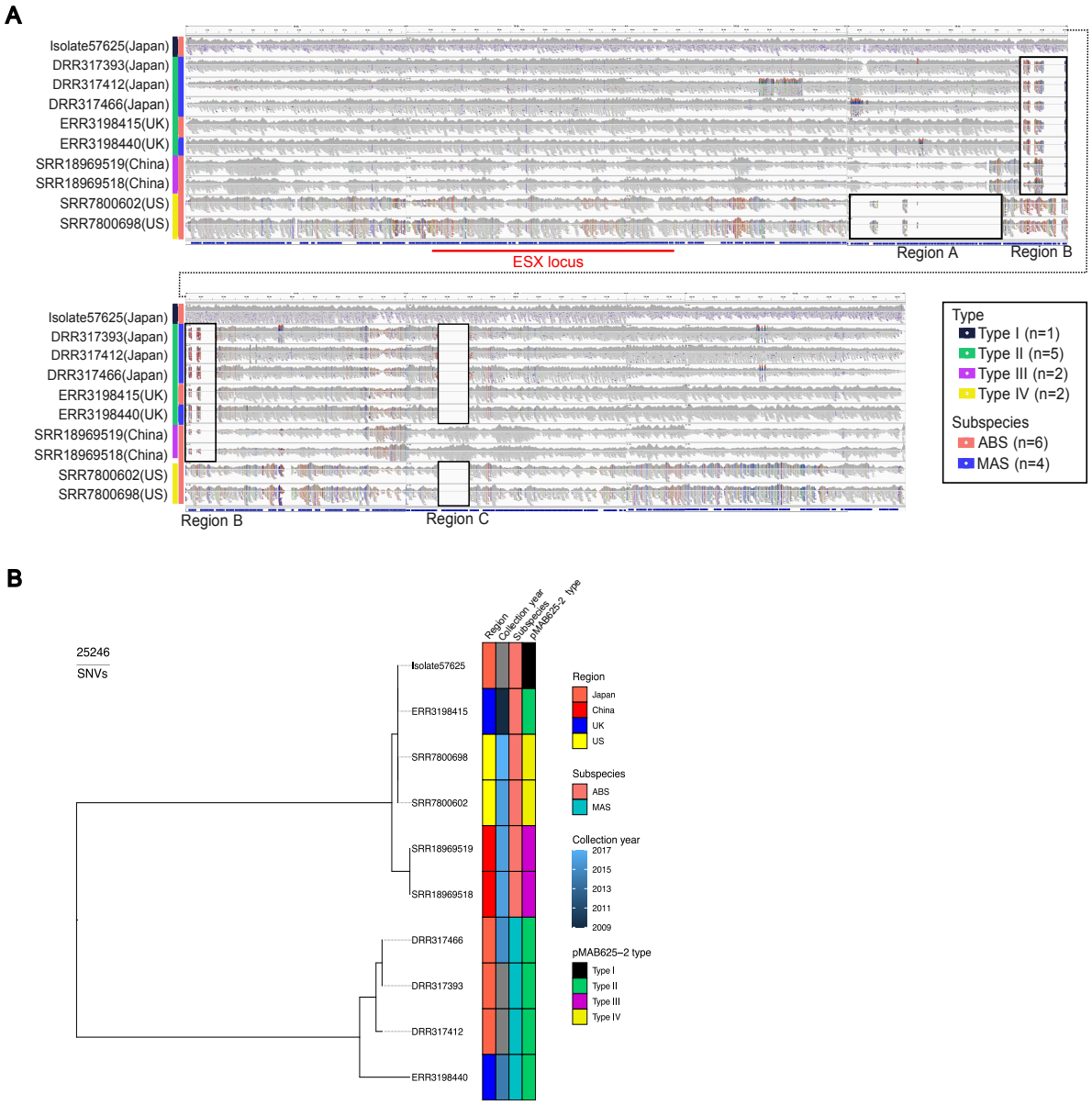

Figure 5. Classification of pMAB625-2 by structural variants and relation with the phylogenetic distance of host bacterial chromosomes

(A) The mapping results of the reads data from each isolate to pMAB625-2 were visualized using IGV. Each sequence was classified into 4 types by the pattern of structural variants (surrounded by black line squares).

(B) Relation between the phylogenetic distance and pMAB625-2 distribution.

DISCUSSION

Plasmids are mobile genetic elements that can move between different bacterial strains and alter host characteristics, such as virulence, and antimicrobial susceptibility. Plasmids are horizontally transferable among bacteria by transformation and conjugation. Thus, plasmid epidemiology, in conjunction with core-

genome analysis, may help to infer past contact between bacteria. In this study, we showed that the multidrug-resistant clinical isolates of ABS isolated from a patient with osteomyelitis had three plasmids (pMAB625-1, pMAB625-2 and pMAB625-3) that the type strain did not harbor. Additionally, analysis of the clinical isolates of *M. abscessus* identified worldwide indicated that pMAB625 plasmids were horizontally transferred between regions and subspecies and that it is sometimes possible to predict past contact between bacteria by tracing the phylogenetic relation of plasmids. Dedrick *et al*. reported that pGD69-1 (pGD69A-1), identical to pMAB625-3, is the same as the other five plasmids[33]. Lewin *et al*. identified pMabs-09-13 through WGS of the clinical isolates of *M. abscessus* within cystic fibrosis patients and reported that pMabs-09-13 exhibits an identity of 99.86% to pGD42-1, pGD69A-1, and pGD69B-1[34]. These reports suggested that pMAB625-3 is spreading among many other isolates of *M. abscessus*, but the detailed distribution of pMAB625 plasmids in the world and other subspecies has remained unclear. Our study shows that pMAB625-3 is the plasmid spreading beyond regions and subspecies in the largest number of clinical isolates of *M. abscessus*. This allowed us to investigate the possibility of speculating the precise classification of bacteria and the past contact between them. The phylogenetic tree analysis of pMAB625-3 based on the SNVs of plasmids (Figure 4A) indicated that the SNV pattern was correlated with the phylogenetic relation of the hosts' chromosome sequences; however, a unique variant (SRR7800511, US) different from the other sequences in the clade was found. This indicates that it is possible to predict the bacterial contact using the distribution of the unique variant like SRR7800511. In the case of pMAB625-2, it is actually indicated that the past contact between the different subspecies is predictable based on the relation between the phylogenetic tree of the hosts' chromosomes and the distribution of pMAB625-2 type.

As important findings, we found that 2.2% (10/462) and 11.5% (53/462) of the clinical isolates worldwide had pMAB625-2, and pMAB625-3, respectively (Table 4). This result provides an epidemiological insight into the spread of plasmids in *M. abscessus* beyond regions and strains. Other than person-to-person transmission of *M.abscessus*, this global spread of pMAB625 plasmids may be mainly due to increased global logistical activity and human mobility with associated interference of human and microbial habitats[35]. The habitat of *M. abscessus* is soil and water systems, and it is also possible that increased flooding due to recent climate change may have increased the chance of contact between the different strains. Analysis of plasmid distribution revealed that some plasmids (pMAB625-2, pMAB625-3, pGD19, pGD25-1 and pGD69A-2) have been widely spread between strains, regions and subspecies, while others (pGD22-2 and pGD42-2) have been restricted to specific strains and regions (Figure 3). Therefore, it is speculated that regarding pGD22-2 and pGD42-2, the identical isolates retaining these plasmids had been spread within or between the regions, whereas, regarding pMAB625-2, pMAB625-3, pGD19, pGD25-1 and p69A-2, plasmids themselves had been spread between different strains, subspecies and region through horizontal transfer. It is unknown what factors determine these differences in plasmid distribution. It is possible that the factors encoded on the plasmid or the periods from the emergence were different among the plasmids. In addition, we also showed the plasmid distribution was different from *M. abscessus* and MAC (Table S8), indicating that incompatibility also exists in the plasmids present in NTM, strictly distinguishing *M. abscessus* from other NTMs except for very few cases, such as pMN23 and pMFLV03.

We identified various factors associated with bacterial virulence and multidrug resistance on the pMAB625 plasmids. The components of the ESX secretion system, the MMPL family transporter, and the components of the TA system were encoded on the plasmids, and these genes were highly expressed in the clinical isolates compared to the type strain. The ESX secretion system is involved in the export of the various pathogenic proteins and metal ions associated with proliferation, survival in the cytosol of macrophage, and conjugation. It has also been reported that ESX-1 components are required for sliding motility and biofilm formation in *M. avium*[20]. Therefore, given the close genetic distance between ESX-1 and ESX-P cluster 5, which include the components of the ESX secretion system on the pMAB625-1 and pMAB625-2 (Figure 1B), the components of ESX-P cluster 5 may be involved in biofilm formation. In addition, MMPL family

transporters can transport antibiotics across the cell membrane. It has been reported that the increased expression of MMPL5 is associated with decreased susceptibility to bedaquiline, and clofazimine in *M. tuberculosis*[36,37], bedaquiline, and clofazimine in *M. intracellulare*[38], and thiactazone derivative in *M. abscessus*[39]. The function of the MMPL family transporter encoded on the pMAB625-3 is unknown; however, the presence of mutational hotspots (Figure 4B) indicates that this MMPL transporter may be compatible with a variety of substrates, including antimicrobial agents. Therefore, our results suggest that Isolate57625 enhanced defence mechanisms against antibiotics through the acquisition of the ESX secretion system and transporters, accompanied by changes in biofilm barriers, and transport of antibiotics. These results suggest that pMAB625 plasmids appeared to be a cause of the low susceptibility to carbapenem antibiotics in the clinical isolates compared with the type strain; however, further studies will be essential to determine whether these plasmids are the main cause of AMR.

In conclusion, we reported the distribution of plasmids in *M. abscessus* and found that pMAB625-3 is the most widely distributed plasmid in the clinical isolates of *M. abscessus* worldwide. In addition, phylogenetic tree analysis and mutational analysis of the pMAB625 plasmids partially predict past bacterial contact. These findings provide a new perspective on the acquisition of genomic diversity, the origin and transmission route of *M. abscessus.* These findings will also lead to the development of effective countermeasures to identify pathways of bacterial transmission and prevent serious bacterial outbreaks.

Limitations of the study

Although it is assumed that phylogenetically close plasmids with similar SNV and SV patterns were spread via bacterial contact, it cannot be excluded that they may have acquired identical mutation patterns in their respective clinical isolates without bacterial contact. To clarify this, it is necessary to calculate the mutation rate of the plasmid and compare the mutation acquisition period with the interval of appearance in the different strains. In addition, future studies are required to verify whether the pMAB625 plasmids induce multidrug resistance in *M. abscessus* by plasmid transfection.

RESOURCE AVAILABILITY

Lead contact

Further information and requests for resources and reagents should be directed to and will be fulfilled by the lead contact, Masashi Toyoda (mtoyoda@tmig.or.jp).

Materials availability

This study did not generate new unique reagents.

Data and code availability

- All raw sequence data generated in this study have been deposited in the DDBJ database at https://www.ddbj.nig.ac.jp/ under the BioProject accession number PRJDB16220. The complete genome sequences of the isolates are available in the DDBJ database. They can be accessed using the accession numbers, AP028613, AP028614, AP028615, and AP028616 for Isolate57625; AP028617, AP028618, AP028619, and AP028620 for Isolate57629; AP028621, AP028622, AP028623, and AP028624 for Isolate57630; AP028625, AP028626, AP028627, and AP028628 for Isolate57596; AP028629, AP028630, AP028631, and AP028632 for Isolate57626, for the chromosome and three plasmids in each isolate.
- The analyzed data of RNA-seq have been deposited in the Genomic Expression Archive at https://www.ddbj.nig.ac.jp/gea/ under the accession number E-GEAD-827.

- All data reported in this paper will be shared by the lead contact upon request.
- This paper does not report original code.

- Any additional information required to reanalyze the data reported in this paper is available from the lead contact upon request.

ACKNOWLEDGMENTS

The authors thank the staff of the microbiology laboratory of Dokkyo Medical University Hospital for performing identification and drug susceptibility tests, and Dr. Yoshishige Masuda and Dr. Takashi Inamatsu at TMIG for supervising in clinical practice. Computations were partially performed on the NIG supercomputer at ROIS National Institute of Genetics. This work was supported by Japan Society for the Promotion of Science (JSPS) KAKENHI Grant Number JP19K08938.

AUTHOR CONTRIBUTIONS

Conceptualization,K.O., A.Y.; Formal analysis, K.O.; Methodology, K.O., A.Y., and Hiroshi Koganemaru; Data curation, K.O.; Investigation,K.O., Keisuke Kamada, and Ken Kikutchi ; Validation, K.O.; Writing-original draft, K.O. and A.Y.; Writing-review & editing, K.O., Y.A. and M.T.; Funding acquisition, A.Y. and Ken Kikuchi.; Patient care and resources, Hironobu Kitazawa, Y.I., T.S. and K.W.; Supervision, M.T.

DECLARATION OF INTERESTS

The authors declare no competing interests.

SUPPLEMENTAL INFORMATION

Document S1. Figures S1–S6
Table S1. Primer sequences used in this study
Table S2. Genbank accession numbers of the genome and plasmid sequences in this study
Table S3. Gene lists on chromosome which were acquired, lost and mutated in Isolate57625 compared with ATCC19977
Table S4. Gene lists which were acquired, lost and mutated in Isolate57625 compared with ATCC19977
Table S5. Homology search results of genes on pMAB625 plasmids against genes of Mycobacterium
Table S6. The results of RNA-seq analysis
Table S7. The mutation type of MMPL family transporter
Table S8. The analysis of distribution regarding NTM plasmids in the clinical isolates of *M. abscessus*

503 **FIGURE TITLES AND LEGENDS**

504 **Figure 1. Phylogenetic and gene expression analysis of the genes related to the ESX secretion**
505 **system**
506 (A) The loci of the ESX secretion system are encoded on pMAB625-1 and pMAB625-2. CDSs of the ESX
507 secretion system were searched using Blast+. The core components that construct membrane pore
508 (*eccB, eccC, eccD, mycP,* and *eccE*) are contained in this operon.
509 (B) Phylogenetic tree analysis of various ESX loci encoded on chromosomes and plasmids. The amino
510 acid sequence of the genes that construct the membrane pore were concatenated and the phylogenetic
511 tree was created by NGphylogeny.fr[24] using the PhyML+SMS inference method. The classification of
512 each cluster was followed as previously reported[21].
513 (C) RNA-seq analysis of the type strain and the isolates. The x-axis represents the mean log expression
514 levels, and the y-axis of the top plot represents the log fold change. The bottom dot plot and box plot
515 represent the distribution of the expression levels of each gene. The green dots represent the data of
516 genes that the isolates acquired by SVs and plasmid acquisition. The red dots represent the data of ESX
517 secretion system genes encoded on the plasmids.
518

519 **Figure 2. The distribution of pMAB625 plasmid in the clinical isolates in Japan**
520 (A) PCR analysis of the possession of pMAB625 plasmid in the clinical isolates which our group isolated
521 in Japan. PCR was performed using the primers specific to each plasmid and *HrpA*. The color bar
522 represents the species of each isolate. The primer sets of *HrpA* were different depending on the species.
523 (B) Mapping the read data of the clinical isolates in Japan to Isolate57625 genome sequence. The bar
524 plot represents the depth of coverage to chromosome and each plasmid and the dot plot represents the
525 percentage of covered genome region.
526 (C) Geographical map of Japan. The prefectures in which the pMAB625 plasmids were detected are
527 represented by color.
528

529 **Figure 3. The relation between the phylogenetic distance of host bacterial chromosomes and**
530 **plasmid distribution in clinical isolates worldwide**

531 The phylogenetic tree was created by Gubbins[27] using chromosome sequences and visualized by
532 ggtree[28]. The read data of the clinical isolates collected worldwide were mapped to pMAB625 and known
533 plasmid sequences to verify the plasmid distribution. Tree-scale represents the number of SNVs per
534 genome.

535

536 **Figure 4 Phylogenetic tree and SNVs analysis of pMAB625-3**

537 (A) Phylogenetic tree of the sequences of pMAB625-3 detected in the 53 isolates. The phylogenetic tree
538 was created using the maximum-likelihood method using iQ-TREE2 based on the core-SNVs data. The
539 sequences belonging to the clade covered by yellow color were identical, although the sequence of
540 SRR18969469 was heterogeneous. The classification of "Clade (Chromosome)" is based on the clade in
541 the phylogenetic tree indicated in Figure 3. pMAB625-3 sequences of the isolates covered by yellow box
542 were identical except for SRR18969469, whose sequence of MMPL family transporter was mixed.

543 (B) The classification of the pMAB625 sequences based on the SNVs. The mapping results of the reads
544 data from each isolate to pMAB625-3 were also visualized by IGV. The mutation hotspot was located at
545 the MMPL family transporter (surrounded by a black line square). The mutation types of the MMPL
546 transporters were classified into three types, and all mutations at this region were missense or silent.

547

548 **Figure 5. Classification of pMAB625-2 by structural variants and relation with the phylogenetic**
549 **distance of host bacterial chromosomes**

550 (A) The mapping results of the reads data from each isolate to pMAB625-2 were visualized using IGV.
551 Each sequence was classified into 4 types by the pattern of structural variants (surrounded by black line
552 squares).

553 (B) Relation between the phylogenetic distance and pMAB625-2 distribution.

554

555

556 ## TABLES AND TEXT BOXES

557 **Table 1. The isolation time point of the clinical isolates and antimicrobial susceptibility of the type**
558 **strain and the isolates**

Isolates	Source	Period from the first isolation (month)	MIC[a] (μg/mL)														
			AMK	TOB	IPM	FRPM	LVFX	MFLX	AZM	CAM 4day	CAM 14day	ST	DOXY	MEPM	LZD	CLF	STFX
ATCC 19977	-	-	8	8	16	>64	32	>8	64	2	>64	>152/8	>16	64	32	1	2
Isolate57625	catheter	0	8	8	16[b]	>64	16	>8	64	2	>64	>152/8	>16	>64	32	1	2
Isolate57629	catheter	4	-	-	-	-	-	-	-	-	-	-	-	-	-	-	-
Isolate57630	bone biopsy	4	-	-	-	-	-	-	-	-	-	-	-	-	-	-	-
Isolate57596	heel	6	-	-	-	-	-	-	-	-	-	-	-	-	-	-	-
Isolate57626	malleolus	6	8	8	>64[c]	>64	32	>8	64	2	>64	>152/8	>16	>64	32	1	2

559 [a]MICs were determined as the minimum concentration at which the bacteria did not grow. No antimicrobial
560 susceptibility testing was conducted on the isolates other than Isolate57625 and Isolate57626, representing hyphens
561 in the table. The test was repeated three times and all MICs were confirmed to be the same between the experiments
562 with the exception of imipenem for the isolates. AMK, Amikacin; TOB, Tobramycin; IPM, Imipenem; FRPM,
563 Faropenem; LVFX, Levofloxacin; MFLX, Moxifloxacin; AZM, Azithromycin; CAM, Clarithromycin; ST,
564 Trimethoprim/sulfamethoxazole; DOXY, Doxycycline; MEPM, Meropenem; LNZ, Linezolid; CLF, Clofazimine; STFX,
565 Sitafloxacin
566 [b]For Isolate57625, the MICs against IPM in the three experiments were 64, 16, and 16 μg/mL, respectively.
567 [c]For Isolate57626, the MICs against IPM in the three experimenst were >64, 16, and >64 μg/mL, respectively.
568

569 **Table 2. Genome assembly and the annotation statics of the Isolate57625**

Contig	Form	Length(bp)	GC contents (%)	Number of CDS	Number of rRNA	Number of tRNA	Number of tmRNA
Chromosome	circular	5,072,346	64.1	5,034	3	48	1
pMAB625-1	linear	202,398	64.7	247	0	29	0
pMAB625-2	linear	142,689	62.2	171	0	0	0
pMAB625-3	circular	24,988	65.6	30	0	0	0

570

571 **Table 3. Homology search result between plasmids identified in *M. abscessus***

Plasmid	Accession no.	Topology	Length (bp)	Homologous plasmid (ANI(%)>99)	Homologous plasmid (97< ANI(%) <99)	Use for "Reference"
pMAB625-1	AP028614.1	linear	202,398	-	-	TRUE
pMAB625-2	AP028615.1	linear	142,689	-	pGD21-2[b]	TRUE
pMAB625-3	AP028616.1	circular	24,988	pGD69A-1, pGD42-1	-	TRUE
pMAB23	NC_010394.1	circular	23,319	pMabS_GZ002[a], FDAARGOS_1604_plasmid	-	TRUE
pMabS_GZ002	NZ_CP034180.1	linear	15,203	pMAB23, FDAARGOS_1604_plasmid	-	TRUE

pGD19	NZ_CP063329.1	circular	18,605	-	-	TRUE
pGD21-1	NZ_CP065285.1	circular	112,633	-	-	TRUE
pGD21-2	NZ_CP065286.1	linear	155,609	-	pMAB625-2[b]	TRUE
pGD22-1	NZ_CP063325.1	circular	19,694	-	-	TRUE
pGD22-2	NZ_CP063326.1	circular	18,117	pGD42-2[a]	-	TRUE
pGD25-1	NZ_CP063321.1	circular	31,413	-	-	TRUE
pGD25-2	NZ_CP063322.1	circular	27,424	-	-	TRUE
pGD25-3	NZ_CP063323.1	circular	23,599	-	-	TRUE
pGD42-1	NZ_CP065281.1	circular	24,993	pMAB625-3, pGD69A-1	-	FALSE
pGD42-2	NZ_CP065282.1	circular	9,547	pGD22-2	pGD69A-2	TRUE
pGD69A-1	NZ_CP065270.1	circular	25,000	pMAB625-3, pGD42-1	-	FALSE
pGD69A-2	NZ_CP065271.1	circular	18,611	-	pGD42-2[a]	TRUE
pJCM30620_1	NZ_AP022622.1	linear	119,389	50594_plasmid2[a]	-	TRUE
pJCM30620_2	NZ_AP022623.1	linear	38,763	50594_plasmid1[b]	-	TRUE
BRA100	NC_017908.2	circular	56,265	-	-	TRUE
FDAARGOS_1604_plasmid	NZ_CP085920.1	circular	23,319	pMAB23, pMabS_GZ002[a]	-	FALSE
50594_plasmid1	NC_021278.1	circular	172,814	pJCM30620_2[a]	-	TRUE
50594_plasmid2	NC_021279.1	circular	97,240	pJCM30620_1[b]	-	TRUE

572 [a]One Structural Variant (SV) exists in the sequence.

573 [b]More than two SVs exist in the sequence.

574

575 **Table 4. pMAB625 and known plasmids distribution in the clinical isolates worldwide**

	Number (%) of isolates retaining plasmid							
Region	Unknown (Type strain)	Japan	China	Taiwan	US	Spain	UK	total[a]
Analyzed isolates	3	125	69	98	110	30	30	462
pMAB625-1	0	1 (0.8)	0	0	0	0	0	1 (0.2)
pMAB625-2	0	4 (3.2)	2 (2.9)	0	2 (1.8)	0	2 (6.7)	10 (2.2)
pMAB625-3	0	16 (12.8)	5 (7.2)	8 (8.2)	14 (12.7)	9 (30.0)	1 (3.3)	53 (11.5)
pMAB23	1 (33.3)	0	0	0	1 (0.9)	0	0	1 (0.2)
pMabS_GZ002	1 (33.3)	0	0	0	1 (0.9)	0	0	1 (0.2)

pGD69A-2	0	0	0	1 (1.0)	9 (8.2)[b]	2 (6.7)	3 (10.0)	15(3.2)
pGD19	0	0	4 (5.8)	3 (3.1)	0	1 (3.3)	1 (3.3)	9(1.9)
pJCM30620_1	0	0	1 (1.4)	0	0	0	1 (3.3)	2(0.4)
50594_plasmid2	0	0	1 (1.4)	0	0	0	1 (3.3)	2(0.4)
pGD22-2	0	0	0	0	6 (5.5)	4 (13.3)[c]	1 (3.3)	11(2.4)
pGD42-2	0	0	0	1 (1.0)	12 (10.9)[d]	4 (13.3)[b]	1 (3.3)	18(3.9)
pGD25-1	0	0	0	0	3 (2.7)	0	4 (13.3)[c]	7(1.5)
pGD25-2	0	0	0	0	1 (0.9)	0	2 (6.7)	3(0.6)

576 Fisher's exact tests were performed to verify regional differences in the frequency of appearance of each
577 plasmid. Corrections for the multiple comparisons were performed using Holm's method.

578 [a]Total number excludes the number of the type strains.

579 [b]$p<0.05$, compared with Japan

580 [c]$p<0.05$, compared with Japan and Taiwan

581 [d]$p<0.05$, compared with Japan, China and Taiwan

582

583

584 **REFERENCES**

585 1. Naghavi, M., Vollset, S.E., Ikuta, K.S., Swetschinski, L.R., Gray, A.P., Wool, E.E., Aguilar, G.R.,
586 Mestrovic, T., Smith, G., Han, C., et al. (2024). Global burden of bacterial antimicrobial resistance 1990–
587 2021: a systematic analysis with forecasts to 2050. The Lancet *404*, 1199–1226.
588 https://doi.org/10.1016/S0140-6736(24)01867-1.

589 2. Johansen, M.D., Herrmann, J.-L., and Kremer, L. (2020). Non-tuberculous mycobacteria and the
590 rise of Mycobacterium abscessus. Nat Rev Microbiol *18*, 392–407. https://doi.org/10.1038/s41579-020-
591 0331-1.

592 3. Cristancho-Rojas, C., Varley, C.D., Lara, S.C., Kherabi, Y., Henkle, E., and Winthrop, K.L. (2024).
593 Epidemiology of *Mycobacterium abscessus*. Clinical Microbiology and Infection *30*, 712–717.
594 https://doi.org/10.1016/j.cmi.2023.08.035.

595 4. Bryant, J.M., Grogono, D.M., Greaves, D., Foweraker, J., Roddick, I., Inns, T., Reacher, M.,
596 Haworth, C.S., Curran, M.D., Harris, S.R., et al. (2013). Whole-genome sequencing to identify
597 transmission of Mycobacterium abscessus between patients with cystic fibrosis: a retrospective cohort
598 study. Lancet *381*, 1551–1560. https://doi.org/10.1016/S0140-6736(13)60632-7.

599 5. Lipworth, S., Hough, N., Weston, N., Muller-Pebody, B., Phin, N., Myers, R., Chapman, S., Flight,
600 W., Alexander, E., Smith, E.G., et al. (2021). Epidemiology of Mycobacterium abscessus in England: an
601 observational study. Lancet Microbe *2*, e498–e507. https://doi.org/10.1016/S2666-5247(21)00128-2.

602 6. Bryant, J.M., Grogono, D.M., Rodriguez-Rincon, D., Everall, I., Brown, K.P., Moreno, P., Verma,
603 D., Hill, E., Drijkoningen, J., Gilligan, P., et al. (2016). Emergence and spread of a human-transmissible
604 multidrug-resistant nontuberculous mycobacterium. Science *354*, 751–757.
605 https://doi.org/10.1126/science.aaf8156.

606 7. Yoshida, M., Chien, J.-Y., Morimoto, K., Kinjo, T., Aono, A., Murase, Y., Fujiwara, K., Morishige,
607 Y., Nagano, H., Jou, R., et al. (2022). Molecular Epidemiological Characteristics of Mycobacterium
608 abscessus Complex Derived from Non-Cystic Fibrosis Patients in Japan and Taiwan. Microbiol Spectr *10*,
609 e00571-22. https://doi.org/10.1128/spectrum.00571-22.

610 8. Davidson, R.M. (2018). A Closer Look at the Genomic Variation of Geographically Diverse
611 Mycobacterium abscessus Clones That Cause Human Infection and Disease. Front Microbiol *9*, 2988.
612 https://doi.org/10.3389/fmicb.2018.02988.

613 9. Zhang, M., Adroub, S., Ummels, R., Asaad, M., Song, L., Pain, A., Bitter, W., Guan, Q., and
614 Abdallah, A.M. (2024). Comprehensive pan-genome analysis of Mycobacterium marinum: insights into
615 genomic diversity, evolution, and pathogenicity. Sci Rep *14*, 27723. https://doi.org/10.1038/s41598-024-
616 75228-0.

617 10. Choo, S.W., Wee, W.Y., Ngeow, Y.F., Mitchell, W., Tan, J.L., Wong, G.J., Zhao, Y., and Xiao, J.
618 (2014). Genomic reconnaissance of clinical isolates of emerging human pathogen Mycobacterium
619 abscessus reveals high evolutionary potential. Sci Rep *4*, 4061. https://doi.org/10.1038/srep04061.

620 11. Bronson, R.A., Gupta, C., Manson, A.L., Nguyen, J.A., Bahadirli-Talbott, A., Parrish, N.M., Earl,
621 A.M., and Cohen, K.A. (2021). Global phylogenomic analyses of Mycobacterium abscessus provide
622 context for non cystic fibrosis infections and the evolution of antibiotic resistance. Nat Commun *12*, 5145.
623 https://doi.org/10.1038/s41467-021-25484-9.

624 12. Sauvage, E., Kerff, F., Terrak, M., Ayala, J.A., and Charlier, P. (2008). The penicillin-binding
625 proteins: structure and role in peptidoglycan biosynthesis. FEMS Microbiol Rev *32*, 234–258.
626 https://doi.org/10.1111/j.1574-6976.2008.00105.x.

13. Hellinger, W.C., and Brewer, N.S. (1991). Imipenem. Mayo Clin Proc *66*, 1074–1081. https://doi.org/10.1016/s0025-6196(12)61732-7.

14. Schmartz, G.P., Hartung, A., Hirsch, P., Kern, F., Fehlmann, T., Müller, R., and Keller, A. (2022). PLSDB: advancing a comprehensive database of bacterial plasmids. Nucleic Acids Research *50*, D273–D278. https://doi.org/10.1093/nar/gkab1111.

15. Paulsen, I.T., Brown, M.H., Littlejohn, T.G., Mitchell, B.A., and Skurray, R.A. (1996). Multidrug resistance proteins QacA and QacB from Staphylococcus aureus: membrane topology and identification of residues involved in substrate specificity. Proceedings of the National Academy of Sciences *93*, 3630–3635. https://doi.org/10.1073/pnas.93.8.3630.

16. Chuanchuen, R., Gaynor, J.B., Karkhoff-Schweizer, R., and Schweizer, H.P. (2005). Molecular Characterization of MexL, the Transcriptional Repressor of the mexJK Multidrug Efflux Operon in Pseudomonas aeruginosa. Antimicrob Agents Chemother *49*, 1844–1851. https://doi.org/10.1128/AAC.49.5.1844-1851.2005.

17. Kapopoulou, A., Lew, J.M., and Cole, S.T. (2011). The MycoBrowser portal: a comprehensive and manually annotated resource for mycobacterial genomes. Tuberculosis (Edinb) *91*, 8–13. https://doi.org/10.1016/j.tube.2010.09.006.

18. Osman, M.M., Shanahan, J.K., Chu, F., Takaki, K.K., Pinckert, M.L., Pagán, A.J., Brosch, R., Conrad, W.H., and Ramakrishnan, L. (2022). The C terminus of the mycobacterium ESX-1 secretion system substrate ESAT-6 is required for phagosomal membrane damage and virulence. Proceedings of the National Academy of Sciences *119*, e2122161119. https://doi.org/10.1073/pnas.2122161119.

19. Laencina, L., Dubois, V., Le Moigne, V., Viljoen, A., Majlessi, L., Pritchard, J., Bernut, A., Piel, L., Roux, A.-L., Gaillard, J.-L., et al. (2018). Identification of genes required for Mycobacterium abscessus growth in vivo with a prominent role of the ESX-4 locus. Proceedings of the National Academy of Sciences *115*, E1002–E1011. https://doi.org/10.1073/pnas.1713195115.

20. Lai, L.-Y., Lin, T.-L., Chen, Y.-Y., Hsieh, P.-F., and Wang, J.-T. (2018). Role of the Mycobacterium marinum ESX-1 Secretion System in Sliding Motility and Biofilm Formation. Frontiers in Microbiology *9*, 1160.

21. Dumas, E., Christina Boritsch, E., Vandenbogaert, M., Rodríguez de la Vega, R.C., Thiberge, J.-M., Caro, V., Gaillard, J.-L., Heym, B., Girard-Misguich, F., Brosch, R., et al. (2016). Mycobacterial Pan-Genome Analysis Suggests Important Role of Plasmids in the Radiation of Type VII Secretion Systems. Genome Biology and Evolution *8*, 387–402. https://doi.org/10.1093/gbe/evw001.

22. Zhou, Z., Xu, L., Zhu, L., Liu, Y., Shuai, X., Lin, Z., and Chen, H. (2021). Metagenomic analysis of microbiota and antibiotic resistome in household activated carbon drinking water purifiers. Environment International *148*, 106394. https://doi.org/10.1016/j.envint.2021.106394.

23. Harms, A., Brodersen, D.E., Mitarai, N., and Gerdes, K. (2018). Toxins, Targets, and Triggers: An Overview of Toxin-Antitoxin Biology. Molecular Cell *70*, 768–784. https://doi.org/10.1016/j.molcel.2018.01.003.

24. Lemoine, F., Correia, D., Lefort, V., Doppelt-Azeroual, O., Mareuil, F., Cohen-Boulakia, S., and Gascuel, O. (2019). NGPhylogeny.fr: new generation phylogenetic services for non-specialists. Nucleic Acids Research *47*, W260–W265. https://doi.org/10.1093/nar/gkz303.

25. Kamada, K., Yoshida, A., Iguchi, S., Arai, Y., Uzawa, Y., Konno, S., Shimojima, M., and Kikuchi, K. (2021). Nationwide surveillance of antimicrobial susceptibility of 509 rapidly growing mycobacteria strains isolated from clinical specimens in Japan. Sci Rep *11*, 12208. https://doi.org/10.1038/s41598-021-91757-4.

671 26. Jin, P., Dai, J., Guo, Y., Wang, X., Lu, J., Zhu, Y., and Yu, F. (2022). Genomic Analysis of
672 Mycobacterium abscessus Complex Isolates from Patients with Pulmonary Infection in China. Microbiol
673 Spectr *10*, e00118-22. https://doi.org/10.1128/spectrum.00118-22.

674 27. Croucher, N.J., Page, A.J., Connor, T.R., Delaney, A.J., Keane, J.A., Bentley, S.D., Parkhill, J.,
675 and Harris, S.R. (2015). Rapid phylogenetic analysis of large samples of recombinant bacterial whole
676 genome sequences using Gubbins. Nucleic Acids Research *43*, e15. https://doi.org/10.1093/nar/gku1196.

677 28. Yu, G., Smith, D.K., Zhu, H., Guan, Y., and Lam, T.T.-Y. (2017). ggtree: an r package for
678 visualization and annotation of phylogenetic trees with their covariates and other associated data.
679 Methods in Ecology and Evolution *8*, 28–36. https://doi.org/10.1111/2041-210X.12628.

680 29. Wetzstein, N., Diricks, M., Anton, T.B., Andres, S., Kuhns, M., Kohl, T.A., Schwarz, C., Lewin, A.,
681 Kehrmann, J., Kahl, B.C., et al. (2024). Clinical and genomic features of Mycobacterium avium complex: a
682 multi-national European study. Genome Med *16*, 86. https://doi.org/10.1186/s13073-024-01359-8.

683 30. Namkoong, H., Kurashima, A., Morimoto, K., Hoshino, Y., Hasegawa, N., Ato, M., and Mitarai, S.
684 (2016). Epidemiology of Pulmonary Nontuberculous Mycobacterial Disease, Japan. Emerging Infectious
685 Diseases *22*, 1116. https://doi.org/10.3201/eid2206.151086.

686 31. Hoefsloot, W., Ingen, J. van, Andrejak, C., Ängeby, K., Bauriaud, R., Bemer, P., Beylis, N.,
687 Boeree, M.J., Cacho, J., Chihota, V., et al. (2013). The geographic diversity of nontuberculous
688 mycobacteria isolated from pulmonary samples: an NTM-NET collaborative study. European Respiratory
689 Journal *42*, 1604–1613. https://doi.org/10.1183/09031936.00149212.

690 32. Stinear, T.P., Seemann, T., Harrison, P.F., Jenkin, G.A., Davies, J.K., Johnson, P.D.R., Abdellah,
691 Z., Arrowsmith, C., Chillingworth, T., Churcher, C., et al. (2008). Insights from the complete genome
692 sequence of Mycobacterium marinum on the evolution of Mycobacterium tuberculosis. Genome Res *18*,
693 729–741. https://doi.org/10.1101/gr.075069.107.

694 33. Dedrick, R.M., Aull, H.G., Jacobs-Sera, D., Garlena, R.A., Russell, D.A., Smith, B.E.,
695 Mahalingam, V., Abad, L., Gauthier, C.H., and Hatfull, G.F. (2021). The Prophage and Plasmid Mobilome
696 as a Likely Driver of Mycobacterium abscessus Diversity. mBio *12*, e03441-20.
697 https://doi.org/10.1128/mBio.03441-20.

698 34. Lewin, A., Kamal, E., Semmler, T., Winter, K., Kaiser, S., Schäfer, H., Mao, L., Eschenhagen, P.,
699 Grehn, C., Bender, J., et al. (2021). Genetic diversification of persistent Mycobacterium abscessus within
700 cystic fibrosis patients. Virulence *12*, 2415–2429. https://doi.org/10.1080/21505594.2021.1959808.

701 35. Castañeda-Barba, S., Top, E.M., and Stalder, T. (2024). Plasmids, a molecular cornerstone of
702 antimicrobial resistance in the One Health era. Nat Rev Microbiol *22*, 18–32.
703 https://doi.org/10.1038/s41579-023-00926-x.

704 36. Andries, K., Villellas, C., Coeck, N., Thys, K., Gevers, T., Vranckx, L., Lounis, N., Jong, B.C. de,
705 and Koul, A. (2014). Acquired Resistance of Mycobacterium tuberculosis to Bedaquiline. PLOS ONE *9*,
706 e102135. https://doi.org/10.1371/journal.pone.0102135.

707 37. Hartkoorn, R.C., Uplekar, S., and Cole, S.T. (2014). Cross-Resistance between Clofazimine and
708 Bedaquiline through Upregulation of MmpL5 in Mycobacterium tuberculosis. Antimicrob Agents
709 Chemother *58*, 2979–2981. https://doi.org/10.1128/AAC.00037-14.

710 38. Alexander, D.C., Vasireddy, R., Vasireddy, S., Philley, J.V., Brown-Elliott, B.A., Perry, B.J.,
711 Griffith, D.E., Benwill, J.L., Cameron, A.D.S., and Wallace, R.J. (2017). Emergence of mmpT5 Variants
712 during Bedaquiline Treatment of Mycobacterium intracellulare Lung Disease. Journal of Clinical
713 Microbiology *55*, 574–584. https://doi.org/10.1128/jcm.02087-16.

714 39. Halloum, I., Viljoen, A., Khanna, V., Craig, D., Bouchier, C., Brosch, R., Coxon, G., and Kremer,
715 L. (2017). Resistance to Thiacetazone Derivatives Active against Mycobacterium abscessus Involves
716 Mutations in the MmpL5 Transcriptional Repressor MAB_4384. Antimicrob Agents Chemother *61*,
717 e02509-16. https://doi.org/10.1128/AAC.02509-16.

718 40. De Coster, W., D'Hert, S., Schultz, D.T., Cruts, M., and Van Broeckhoven, C. (2018). NanoPack:
719 visualizing and processing long-read sequencing data. Bioinformatics *34*, 2666–2669.
720 https://doi.org/10.1093/bioinformatics/bty149.

721 41. Wick, R.R., Judd, L.M., Gorrie, C.L., and Holt, K.E. (2017). Completing bacterial genome
722 assemblies with multiplex MinION sequencing. Microb Genom *3*, e000132.
723 https://doi.org/10.1099/mgen.0.000132.

724 42. Wang, J.R., Holt, J., McMillan, L., and Jones, C.D. (2018). FMLRC: Hybrid long read error
725 correction using an FM-index. BMC Bioinformatics *19*, 50. https://doi.org/10.1186/s12859-018-2051-3.

726 43. Kolmogorov, M., Yuan, J., Lin, Y., and Pevzner, P.A. (2019). Assembly of long, error-prone reads
727 using repeat graphs. Nat Biotechnol *37*, 540–546. https://doi.org/10.1038/s41587-019-0072-8.

728 44. Walker, B.J., Abeel, T., Shea, T., Priest, M., Abouelliel, A., Sakthikumar, S., Cuomo, C.A., Zeng,
729 Q., Wortman, J., Young, S.K., et al. (2014). Pilon: An Integrated Tool for Comprehensive Microbial Variant
730 Detection and Genome Assembly Improvement. PLOS ONE *9*, e112963.
731 https://doi.org/10.1371/journal.pone.0112963.

732 45. Gurevich, A., Saveliev, V., Vyahhi, N., and Tesler, G. (2013). QUAST: quality assessment tool for
733 genome assemblies. Bioinformatics *29*, 1072–1075. https://doi.org/10.1093/bioinformatics/btt086.

734 46. Wick, R.R., Schultz, M.B., Zobel, J., and Holt, K.E. (2015). Bandage: interactive visualization of
735 de novo genome assemblies. Bioinformatics *31*, 3350–3352.
736 https://doi.org/10.1093/bioinformatics/btv383.

737 47. Tanizawa, Y., Fujisawa, T., and Nakamura, Y. (2018). DFAST: a flexible prokaryotic genome
738 annotation pipeline for faster genome publication. Bioinformatics *34*, 1037–1039.
739 https://doi.org/10.1093/bioinformatics/btx713.

740 48. Tanizawa, Y., Fujisawa, T., Kaminuma, E., Nakamura, Y., and Arita, M. (2016). DFAST and
741 DAGA: web-based integrated genome annotation tools and resources. Bioscience of Microbiota, Food
742 and Health *35*, 173–184. https://doi.org/10.12938/bmfh.16-003.

743 49. Jain, C., Rodriguez-R, L.M., Phillippy, A.M., Konstantinidis, K.T., and Aluru, S. (2018). High
744 throughput ANI analysis of 90K prokaryotic genomes reveals clear species boundaries. Nat Commun *9*,
745 5114. https://doi.org/10.1038/s41467-018-07641-9.

746 50. Darling, A.C.E., Mau, B., Blattner, F.R., and Perna, N.T. (2004). Mauve: Multiple Alignment of
747 Conserved Genomic Sequence With Rearrangements. Genome Res *14*, 1394–1403.
748 https://doi.org/10.1101/gr.2289704.

749 51. Li, H. (2013). Aligning sequence reads, clone sequences and assembly contigs with BWA-MEM.
750 Preprint at arXiv, https://doi.org/10.48550/arXiv.1303.3997 https://doi.org/10.48550/arXiv.1303.3997.

751 52. Danecek, P., Bonfield, J.K., Liddle, J., Marshall, J., Ohan, V., Pollard, M.O., Whitwham, A.,
752 Keane, T., McCarthy, S.A., Davies, R.M., et al. (2021). Twelve years of SAMtools and BCFtools.
753 Gigascience *10*, giab008. https://doi.org/10.1093/gigascience/giab008.

754 53. Garrison, E., and Marth, G. (2012). Haplotype-based variant detection from short-read
755 sequencing. Preprint at arXiv, https://doi.org/10.48550/arXiv.1207.3907.

54. Cingolani, P., Platts, A., Wang, L.L., Coon, M., Nguyen, T., Wang, L., Land, S.J., Lu, X., and Ruden, D.M. (2012). A program for annotating and predicting the effects of single nucleotide polymorphisms, SnpEff: SNPs in the genome of Drosophila melanogaster strain w ^{1118} ; iso-2; iso-3. Fly *6*, 80–92. https://doi.org/10.4161/fly.19695.

55. Robinson, J.T., Thorvaldsdóttir, H., Winckler, W., Guttman, M., Lander, E.S., Getz, G., and Mesirov, J.P. (2011). Integrative genomics viewer. Nat Biotechnol *29*, 24–26. https://doi.org/10.1038/nbt.1754.

56. Li, H. (2018). Minimap2: pairwise alignment for nucleotide sequences. Bioinformatics *34*, 3094–3100. https://doi.org/10.1093/bioinformatics/bty191.

57. Langmead, B., and Salzberg, S.L. (2012). Fast gapped-read alignment with Bowtie 2. Nat Methods *9*, 357–359. https://doi.org/10.1038/nmeth.1923.

58. Anders, S., Pyl, P.T., and Huber, W. (2015). HTSeq—a Python framework to work with high-throughput sequencing data. Bioinformatics *31*, 166–169. https://doi.org/10.1093/bioinformatics/btu638.

59. Sun, J., Nishiyama, T., Shimizu, K., and Kadota, K. (2013). TCC: an R package for comparing tag count data with robust normalization strategies. BMC Bioinformatics *14*, 219. https://doi.org/10.1186/1471-2105-14-219.

60. Minh, B.Q., Schmidt, H.A., Chernomor, O., Schrempf, D., Woodhams, M.D., von Haeseler, A., and Lanfear, R. (2020). IQ-TREE 2: New Models and Efficient Methods for Phylogenetic Inference in the Genomic Era. Molecular Biology and Evolution *37*, 1530–1534. https://doi.org/10.1093/molbev/msaa015.

61. Letunic, I., and Bork, P. (2021). Interactive Tree Of Life (iTOL) v5: an online tool for phylogenetic tree display and annotation. Nucleic Acids Research *49*, W293–W296. https://doi.org/10.1093/nar/gkab301.

62. Chen, S. (2023). Ultrafast one-pass FASTQ data preprocessing, quality control, and deduplication using fastp. iMeta *2*, e107. https://doi.org/10.1002/imt2.107.

63. Shen, W., Le, S., Li, Y., and Hu, F. (2016). SeqKit: A Cross-Platform and Ultrafast Toolkit for FASTA/Q File Manipulation. PLoS ONE *11*, e0163962. https://doi.org/10.1371/journal.pone.0163962.

64. Quinlan, A.R., and Hall, I.M. (2010). BEDTools: a flexible suite of utilities for comparing genomic features. Bioinformatics *26*, 841–842. https://doi.org/10.1093/bioinformatics/btq033.

65. Clinical & Laboratory Standards Institute (2018). Susceptibility Testing of Mycobacteria, Nocardia spp., and Other Aerobic Actinomycetes, M24Ed3E, (CLSI Publication).

66. Bouso, J.M., and Planet, P.J. (2019). Complete nontuberculous mycobacteria whole genomes using an optimized DNA extraction protocol for long-read sequencing. BMC Genomics *20*, 793. https://doi.org/10.1186/s12864-019-6134-y.

67. Camacho, C., Coulouris, G., Avagyan, V., Ma, N., Papadopoulos, J., Bealer, K., and Madden, T.L. (2009). BLAST+: architecture and applications. BMC Bioinformatics *10*, 421. https://doi.org/10.1186/1471-2105-10-421.

68. Feldgarden, M., Brover, V., Haft, D.H., Prasad, A.B., Slotta, D.J., Tolstoy, I., Tyson, G.H., Zhao, S., Hsu, C.-H., McDermott, P.F., et al. (2019). Validating the AMRFinder Tool and Resistance Gene Database by Using Antimicrobial Resistance Genotype-Phenotype Correlations in a Collection of Isolates. Antimicrob Agents Chemother *63*, e00483-19. https://doi.org/10.1128/AAC.00483-19.

69. Jia, B., Raphenya, A.R., Alcock, B., Waglechner, N., Guo, P., Tsang, K.K., Lago, B.A., Dave, B.M., Pereira, S., Sharma, A.N., et al. (2017). CARD 2017: expansion and model-centric curation of the

798 comprehensive antibiotic resistance database. Nucleic Acids Research *45*, D566–D573.
799 https://doi.org/10.1093/nar/gkw1004.

800 70. Zankari, E., Hasman, H., Cosentino, S., Vestergaard, M., Rasmussen, S., Lund, O., Aarestrup,
801 F.M., and Larsen, M.V. (2012). Identification of acquired antimicrobial resistance genes. Journal of
802 Antimicrobial Chemotherapy *67*, 2640–2644. https://doi.org/10.1093/jac/dks261.

803 71. Gupta, S.K., Padmanabhan, B.R., Diene, S.M., Lopez-Rojas, R., Kempf, M., Landraud, L., and
804 Rolain, J.-M. (2014). ARG-ANNOT, a New Bioinformatic Tool To Discover Antibiotic Resistance Genes in
805 Bacterial Genomes. Antimicrobial Agents and Chemotherapy *58*, 212–220.
806 https://doi.org/10.1128/AAC.01310-13.

807 72. Chen, L., Zheng, D., Liu, B., Yang, J., and Jin, Q. (2016). VFDB 2016: hierarchical and refined
808 dataset for big data analysis—10 years on. Nucleic Acids Research *44*, D694–D697.
809 https://doi.org/10.1093/nar/gkv1239.

810 73. Carattoli, A., Zankari, E., García-Fernández, A., Voldby Larsen, M., Lund, O., Villa, L., Møller
811 Aarestrup, F., and Hasman, H. (2014). In Silico Detection and Typing of Plasmids using PlasmidFinder
812 and Plasmid Multilocus Sequence Typing. Antimicrobial Agents and Chemotherapy *58*, 3895–3903.
813 https://doi.org/10.1128/AAC.02412-14.

814 74. Ingle, D.J., Valcanis, M., Kuzevski, A., Tauschek, M., Inouye, M., Stinear, T., Levine, M.M.,
815 Robins-Browne, R.M., and Holt, K.E. (2016). In silico serotyping of E. coli from short read data identifies
816 limited novel O-loci but extensive diversity of O:H serotype combinations within and between pathogenic
817 lineages. Microb Genom *2*, e000064. https://doi.org/10.1099/mgen.0.000064.

818 75. Doster, E., Lakin, S.M., Dean, C.J., Wolfe, C., Young, J.G., Boucher, C., Belk, K.E., Noyes, N.R.,
819 and Morley, P.S. (2020). MEGARes 2.0: a database for classification of antimicrobial drug, biocide and
820 metal resistance determinants in metagenomic sequence data. Nucleic Acids Research *48*, D561–D569.
821 https://doi.org/10.1093/nar/gkz1010.

822 76. Sun, J., Nishiyama, T., Shimizu, K., and Kadota, K. (2013). TCC: an R package for comparing tag
823 count data with robust normalization strategies. BMC Bioinformatics *14*, 219.
824 https://doi.org/10.1186/1471-2105-14-219.

825 77. García-Alcalde, F., Okonechnikov, K., Carbonell, J., Cruz, L.M., Götz, S., Tarazona, S., Dopazo,
826 J., Meyer, T.F., and Conesa, A. (2012). Qualimap: evaluating next-generation sequencing alignment data.
827 Bioinformatics *28*, 2678–2679. https://doi.org/10.1093/bioinformatics/bts503.

828

829

830 **STAR★METHODS**

831 **KEY RESOURCES TABLE**

REAGENT OR RESOURCE	SOURCE	IDENTIFIER
Bacterial and virus strains		
M. abscessus subsp. *abscessus* type strain, ATCC 19977	ATCC	19977
M. abscessus subsp. *massiliense* type strain, JCM 15300	Japan Collection of Microorganisms (JCM), RIKEN BRC	15300
M. abscessus subsp. *bolletii* type strain, JCM 15297	JCM, RIKEN BRC	15297
Isolate57625, Isolate57629, Isolate57630, Isolate57596, and Isolate57626	This study	N/A
Chemicals, peptides, and recombinant proteins		
Trypticase soy agar with 5% sheep blood	Beckton Dickinson	Cat.# 251239
BBL™ Mueller Hinton II Broth (Cation-Adjusted)	Beckton Dickinson	Cat.# 212322
Middlebrook 7H9 Medium	Sigma-Adlrich	Cat.# M0178
2% OGAWA medium	Kyokuto Pharmaceutical Industrial	Cat.# 551-08026
Lysozyme	Sigma-Aldrich	Cat.# L4919
Critical commercial assays		
BrothMIC RGM	Kyokuto Pharmaceutical Industrial	Cat.# 551-10087
EZ-Beads	Promega	Cat.# AMR76813M
Wizard® HMW DNA Extraction Kit	Promega	Cat.# A2920
Qubit™ BR DNA Quantitation Kit	Thermo Fisher Scientific	Cat.# Q32850
Ion Xpress™ Plus Fragment Library Kit	Thermo Fisher Scientific	Cat.# 4471252
Ion Xpress™ Barcode Adapters 1-16 kit	Thermo Fisher Scientific	Cat.# 4471250
TaqMan™ Quantitation Kit	Thermo Fisher Scientific	Cat.# 4468802
Ion PI™ Chip kit v3	Thermo Fisher Scientific	Cat.# A26711
UltraPure™ DNase/RNase-free Distilled Water	Thermo Fisher Scientific	Cat.# 10977015
SUPERase-In™ RNase Inhibitor	Thermo Fisher Scientific	Cat.# AM2696
mirVana™ miRNA Isolation Kit	Thermo Fisher Scientific	Cat.# AM1561
IonXpress™ RNA-Seq Barcode 1-16 Kit	Thermo Fisher Scientific	Cat.# 4475485
Ion PI™ Hi-Q™ OT2 200 Kit v2	Thermo Fisher Scientific	Cat.# A26434
Ion Total RNA-Seq Kit v2	Thermo Fisher Scientific	Cat.# 4479789
PowerUp™ SYBR™ Green Master Mix	Thermo Fisher Scientific	Cat.# A25741
KOD One® PCR Master Mix	TOYOBO	Cat.#LMM-101
Short Read Eliminator Kit	PacBio	Cat.# 102-208-300
Ligation Sequencing Kit	Oxford Nanopore Technologies	Cat.# SQK-LSK109
Native Barcoding Expansion 1-12	Oxford Nanopore Technologies	Cat.# EXP-NBD104
Flow cell (R9.4.1)	Oxford Nanopore Technologies	Cat.# FLO-MIN106

NEBNext® rRNA Depletion Kit (Bacteria)	NEB	Cat.# E7850
Deposited data		
All raw sequence data generated in this study	DDBJ	PRJDB16220
Complete genome sequences (Chromosome, pMAB625-1, pMAB625-2 and pMAB625-3) of the Isolate57625	DDBJ	AP028613 AP028614 AP028615 AP028616
The analyzed RNA-seq data	Genomic Expression Archive (GEA)	E-GEAD-827
Oligonucleotides		
Forward primer for validation of large deletion in Figure S1 for Deletion_1, CAAGAACTGATGGCTGAAATCCTAATG	This study	N/A
Reverse primer for validation of large deletion in Figure S1 for Deletion_1, AAAGTGATGCTTGCTCTGCCAGTC	This study	N/A
Forward primer for validation of large deletion in Figure S1 for Insertion_1, GTTAGATATGTGCAGGAGTTCCGAGTG	This study	N/A
Reverse primer for validation of large deletion in Figure S1 for Insertion_1, ACCAATACTGCCGAATTCTCTAAAAGC	This study	N/A
Forward primer for validation of large deletion in Figure S1 for Insertion_2, GTGACATGATCTTGCTGCTCAAAAG	This study	N/A
Reverse primer for validation of large deletion in Figure S1 for Insertion_2, GCTATCTGTCGCAGTACTTCGTGACC	This study	N/A
Forward Primers for plasmid copy number analysis in Figure S5 for *HrpA* (MAB), GGATCTGGTCCACAAGACCTACAG	This study	N/A
Reverse Primers for plasmid copy number analysis in Figure S5 for *HrpA* (MAB), AAAGTGATGCTTGCTCTGCCAGTC	This study	N/A
Forward Primers for plasmid copy number analysis in Figure S5 for *HrpA* (no MAB), ACCCTGGTGAAGTTGATGACCGAC	This study	N/A
Reverse Primers for plasmid copy number analysis in Figure S5 for *HrpA* (no MAB), AGGAGGAAGTCGATGTTGAGGCTG	This study	N/A
Forward Primers for plasmid copy number analysis in Figure S5 for pMAB625-1(LOCUS_52450), TCTACTACGCAGACCCTGCACATATC	This study	N/A
Reverse Primers for plasmid copy number analysis in Figure S5 for pMAB625-1(LOCUS_52450), AACTGCTGCCACATCGCTTTCTG	This study	N/A
Forward Primers for plasmid copy number analysis in Figure S5 for pMAB625-2(LOCUS_53740), GACCGATCACGTCATCATTCCTAATC	This study	N/A
Reverse Primers for plasmid copy number analysis in Figure S5 for pMAB625-2(LOCUS_53740), GAACCTCAGCCTCAATATGCTCCTC	This study	N/A
Forward Primers for plasmid copy number analysis in Figure S5 for pMAB625-3(LOCUS_54770), CGACCAGGTACACATCCTGACCAC	This study	N/A
Reverse Primers for plasmid copy number analysis in Figure S5 for pMAB625-3(LOCUS_54770), GAGTTGGCTGATTCCGTCTTGGAG	This study	N/A
Software and algorithms		
R (ver. 4.3.1)	R Core Team (2024)	https://www.R-project.org/
MinKNOW (ver.21.06.0)	Oxford Nanopore Technologies	https://nanoporetech.com/
Guppy (ver. 5.0.7)	Oxford Nanopore Technologies	https://nanoporetech.com/
NanoPlot (ver. 1.38.0)	De Coster et al.[40]	https://github.com/wdecoster/NanoPlot

Porechop (ver. 0.2.4)	Wick et al[41]	https://github.com/rrwick/Porechop
Filtlong (ver. 0.2.1)	Wick	https://github.com/rrwick/Filtlong
Fmlrc (ver. 1.0.0)	Wang et al.[42]	https://github.com/holtjma/fmlrc
Flye (ver. 2.9-b1768)	Kolmogorov et al.[43]	https://github.com/mikolmogorov/Flye
Pilon (ver. 1.24.0)	Walker et al.[44]	https://github.com/broadinstitute/pilon
QUAST (ver. 5.0.2)	Gurevich et al.[45]	https://quast.sourceforge.net/
Bandage (ver. 0.8.1)	Wick et al.[46]	https://rrwick.github.io/Bandage/
DFAST (ver.1.5.0)	Tanizawa et al.[47,48]	https://dfast.ddbj.nig.ac.jp/
FastANI (ver.1.34)	Jain et al.[49]	https://github.com/ParBLiSS/FastANI
Mauve (ver. 2.4.0)	Darling et al.[50]	https://darlinglab.org/mauve/mauve.html
Abricate (ver.1.0.1)	Seeman. T	https://github.com/tseemann/abricate
BWA-MEM (ver. 0.7.17-r1188)	Li H.[51]	https://github.com/lh3/bwa
Samtools (ver.1.12)	Danecek et al.[52]	https://github.com/samtools/samtools
Freebayes (ver. 1.3.5)	Garrison et al.[53]	https://github.com/freebayes/freebayes
SnpEff (ver. 5.2)	Cingolani et al.[54]	https://pcingola.github.io/SnpEff/
IGV (ver.2.17.4)	Robinson et al.[55]	https://igv.org/
Minimap2 (ver. 2.21-r1071)	Li H.[56]	https://github.com/lh3/minimap2
Bowtie2 (ver. 2.5.4)	Langmead and Salzberg[57]	https://github.com/BenLangmead/bowtie2
HTseq (ver. 1.99.2)	Anders et al.[58]	https://github.com/htseq/htseq
R package, TCC (ver. 1.26.0)	Sun et al.[59]	https://bioconductor.org/packages/release/bioc/html/TCC.html
Snippy (ver. 4.6.0)	Seeman. T	https://github.com/tseemann/snippy
IQ-TREE (ver.2)	Minh et al.[60]	https://www.iqtree.org
iTOL ver.6.7	Letunic and Bork[61]	https://itol.embl.de
NGphylogeny.fr	Lemoine et al.[24]	https://ngphylogeny.fr
Fastp (ver. 0.23.4)	Chen[62]	https://github.com/OpenGene/fastp
Seqkit ver.2.4.0	Shen et al.[63]	https://github.com/shenwei356/seqkit
Bedtools ver. 2.30.0	Quinlan and Hall[64]	https://github.com/arq5x/bedtools2
Gubbins ver.3.3.1	Croucher[27]	https://github.com/nickjcroucher/gubbins

R package, ggtree (ver 3.10.1)	Yu et al.[28]	https://bioconductor.org/packages/release/bioc/html/ggtree.html
R package, RVAideMemoire (ver. 0.9-83-7)	Herve M.	https://github.com/cran/RVAideMemoire

832

833 ## EXPERIMENTAL MODEL AND STUDY PARTICIPANT DETAILS

834 ### *Clinical isolates and type strain*

835 Ethical approval for this study was obtained from the Ethics Committee of Dokkyo Medical University
836 (approval number 28045). Regarding Isolate57625, Isolate57629, Isolate57630, Isolate57596, and
837 Isolate57626, specimens were obtained from a patient with osteomyelitis at the five time points in six
838 months indicated in Table 1. Each strain was isolated from the specimen at Shizuoka Children's Hospital
839 for diagnosis. The other clinical isolates used for PCR or WGS were stored at Tokyo Metropolitan Institute
840 for Geriatrics and Gerontology or Tokyo Women's Medical University or Dokkyo Medical University[25]. The
841 type strain of ABS, ATCC 19977, was purchased from ATCC (Manassas, VA, US). The type strain of MAS,
842 JCM 15300, and the type strain of BOL, JCM 15297, were provided by Japan Collection of Microorganisms,
843 RIKEN BRC which is participating in the National BioResource Project of the MEXT, Japan.
844

845 ## METHOD DETAILS

846 ### *Growth curve*

847 The type strain and the five clinical isolates were inoculated onto trypticase soy agar with 5% sheep blood
848 (Beckton Dickinson, Franklin Lakes, NJ, US) and incubated at 30 °C for five days. Next, some colonies
849 were inoculated into BBL™ Mueller Hinton II Broth (Cation-Adjusted) (Beckton Dickinson) and incubated
850 overnight at 30°C. These culture media were measured for absorbance (OD_{600}), from which they were
851 prepared to 0.1 by medium. Seventy microliter of the adjusted culture solution was inoculated into 7 mL of
852 BBL™ Mueller Hinton II Broth (Cation-Adjusted) and incubated at 30 °C for eight days with agitation (200
853 rpm). OD_{600} was measured on days one to eight after inoculation. Statistical analysis was performed using
854 R ver. 4.3.1.
855

856 ### *Antimicrobial susceptibility testing*

857 The type strain and the clinical isolates were subcultured on 2% OGAWA medium (Kyokuto Pharmaceutical
858 Industrial, Tokyo, Japan) at 30 °C for five days. Antimicrobial susceptibility testing was performed using
859 BrothMIC RGM (Kyokuto Pharmaceutical Industrial) following CLSI M24 3rd ed[65]. MICs were determined
860 as the minimum concentration at which bacteria had not grown on day four (all antibiotics) and day 14
861 (clarithromycin). The test was repeated three times and all MICs were confirmed to be the same between
862 the experiments, except for imipenem (IPM) for the isolates. For IPM, the MICs of the type strain were
863 confirmed to be the same between all three experiments, while for the MICs of Isolate57625 and
864 Isolate57626, they were confirmed to be the same between two out of three experiments, as indicated in
865 Table 1.
866

867 ### *Mycobacterial DNA isolation and whole-genome sequencing*

868 The type strain and the clinical isolates of *M. abscessus* were stored in frozen stock containing skim milk
869 and 5% (v/v) glycerol. Each strain was inoculated from frozen stocks into Middlebrook 7H9 Medium (Sigma-
870 Aldrich, St. Louis, MO, US) containing 10% (v/v) oleic acid-albumin-dextrose-catalase and 0.2% (v/v)
871 glycerol and cultured at 30 °C for six days with agitation (200 rpm). Bacterial genomic DNA for short-read
872 sequencing was extracted as previously reported[66]. The quality of the extracted DNA was confirmed by
873 agarose gel electrophoresis, and the concentration was measured using Qubit™ BR DNA Quantitation Kit
874 (Thermo Fisher Scientific, Waltham, MA, US). Genomic DNA was fragmented, and the sequencing library
875 was prepared using the Ion Xpress™ Plus Fragment Library Kit and the Ion Xpress™ Barcode Adapters 1-
876 16 kit (Thermo Fisher Scientific) according to the manufacturer's instructions. The quantity of sequencing
877 library was assessed using the Ion Library TaqMan™ Quantitation Kit (Thermo Fisher Scientific). Emulsion
878 PCR for sequence template synthesis was performed with the Ion PI™ Hi-Q™ OT2 200 Kit v2 using the

879 Ion One Touch™ II System and the Ion One Touch™ II ES (Thermo Fisher Scientific). Sequencing was
880 performed using the Ion PI™ Chip kit v3 and the Ion Proton™ System (Thermo Fisher Scientific). Data were
881 collected using the Torrent Suite v5.0.5 software (Thermo Fisher Scientific).

882

883 High-molecular-weight genomic DNA for long-read sequencing was extracted as follows. The bacterial
884 pellet was collected by centrifugation and homogenized using EZ-beads (Promega, Madison, WI, US) and
885 Shakeman 6 (Bio Medical Science, Tokyo, Japan). The homogenized pellet was lysed with Lysozyme
886 (Sigma-Aldrich) at 37 °C for one hour. Next, DNA was extracted using Wizard® HMW DNA Extraction Kit
887 (Promega) following the manufacturer's instructions. Fragmented DNA in the extracted DNA was removed
888 using the Short Read Eliminator Kit (PacBio, Menlo Park, CA, US). The sequencing library for long-read
889 sequencing was prepared using the Ligation Sequencing Kit (SQK-LSK109, Oxford Nanopore
890 Technologies, Oxford, UK) and the Native Barcoding Expansion 1-12 (EXP-NBD104, Oxford Nanopore
891 Technologies). In brief, the barcode sequences for multiplex sequencing were attached to the ends of the
892 HMW genomic DNA. In addition, the sequencing adapters were ligated to the end of HMW genomic DNA.
893 The prepared DNA was loaded into a flow cell (FLO-MIN106, Oxford Nanopore Technologies) attached to
894 MinION Mk1B (Oxford Nanopore Technologies). Sequencing data were acquired using MinKNOW
895 ver.21.06.0 (Oxford Nanopore Technologies), and base calling was performed using Guppy ver. 5.0.7
896 (Oxford Nanopore Technologies) with high accuracy mode using the National Institute of Genomics
897 supercomputer system (NIG, Shizuoka, Japan). Data quality was confirmed using NanoPlot ver. 1.38.0[40]
898 and adapter sequences were trimmed using Porechop ver. 0.2.4[41]. Raw reads shorter than 1000 bp
899 (Isolate57625, Isolate57629, Isolate57630, Isolate57596) or 5000 bp (Isolate57626) were removed using
900 Filtlong ver. 0.2.1 (https://github.com/rrwick/Filtlong). Filtered reads were corrected using Fmlrc ver. 1.0.0[42]
901 with the data of short-read sequencing acquired by the Ion Proton™ Sequencer. *De novo* assembly was
902 performed using Flye ver. 2.9-b1768[43] with corrected long-reads. Assembled genome sequences were
903 polished using Pilon ver. 1.24.0[44], evaluated using QUAST ver. 5.0.2[45], and visualized using Bandage ver.
904 0.8.1[46]. Genome annotation was performed using DFAST ver.1.5.0[47,48].

905

906 ***Plasmid sequence analysis***

907 Known plasmid sequences were downloaded from PLSDB[14] by the taxonomic search for "*abscessus*".
908 Average nucleotide identity (ANI) was calculated using FastANI ver.1.34[49] and structural variants (SVs)
909 were analyzed using Mauve ver. 2.4.0[50].

910

911 Homology search was performed by blast+[67] using the amino acid sequence as the query or by Abricate
912 ver.1.0.1 (http://github.com/tseemann/abricate) using the nucleotide sequences as the query. NCBI
913 AMRFinderPlus[68], CARD[69], Resfinder[70], ARG-ANNOT[71], VFDB[72], PlasmidFinder[73], EcOH[74], and
914 MEGARes 2.00[75] were used as the database for the search of AMR genes. Mycobrowser[17] was used as
915 the database for the homology search of the mycobacterium genes.

916

917 ***SNVs and SVs analysis***
918 Short-read data acquired by the Ion Proton™ Sequencer were mapped using BWA-MEM ver. 0.7.17-
919 r1188[51] against the reference sequence (CU458896.1, CU458745.1). Output BAM files were sorted using
920 samtools ver.1.12[52]. Valiant calling was performed using Freebayes ver. 1.3.5[53], and variants were
921 annotated using SnpEff ver. 5.2[54] with annotated genome sequence. The positions of single nucleotide
922 variants (SNVs) were visualized using IGV[55] (Broad Institute, Cambridge, MA, US). Assembled genome
923 sequences were aligned using Mauve ver. 2.4.0[50] for SVs analysis. Mapping the short- and long-read to

924 the assembled genome sequence using minimap2 ver. 2.21-r1071[56] was performed for the validation of
925 assembly.

926

927 PCR for the validation of SVs was performed using KOD One® PCR Master Mix (TOYOBO, Osaka, Japan)
928 and the primers indicated in Table S1. Amplified DNA was confirmed using agarose gel electrophoresis
929 following staining with SYBR™ Safe Gel Stain (Thermo Fisher Scientific).

930

931 ***RNA-seq analysis***

932 Total RNA was extracted as follows: The bacterial pellet was collected by centrifugation and suspended in
933 UltraPure™ DNase/RNase-free Distilled Water (Thermo Fisher Scientific) and homogenized using EZ-
934 beads (Promega) and Shakeman 6 (Bio Medical Science). SUPERase-In™ RNase Inhibitor (Thermo Fisher
935 Scientific) was added to the homogenized pellet. Next, the homogenized pellet was lysed by Lysozyme
936 (Sigma-Aldrich) at 37 °C for an hour. Total RNA was purified by mirVana™ miRNA Isolation Kit (Thermo
937 Fisher Scientific). The size and quality of total RNA were assessed using the Agilent 2100 Bioanalyzer
938 (Agilent Technologies, Santa Clara, CA, US) and the RNA 6000 Nano Kit (Agilent Technologies). rRNA
939 was depleted using the NEBNext® rRNA Depletion Kit (Bacteria) (NEB, Ipswich, MA, US) from 500 ng of
940 total RNA. The whole transcriptome library was prepared using the Ion Total RNA-Seq Kit v2 (Thermo
941 Fisher Scientific) as follows: First, the rRNA-depleted RNA was fragmented by RNase III at 37 ˚C for 10
942 minutes and purified using the Magnetic Beads Cleanup Module. Next, adapter sequences were ligated
943 and reverse transcription was performed. The whole transcriptome library was amplified and barcoded
944 using the IonXpress™ RNA-Seq Barcode 1-16 Kit (Thermo Fisher Scientific). The quantity of the amplified
945 whole transcriptome library was assessed using the Ion Library TaqMan™ Quantitation Kit (Thermo Fisher
946 Scientific). Emulsion PCR for sequence template synthesis was performed using the Ion PI™ Hi-Q™ OT2
947 200 Kit v2 with the Ion One Touch™ II System and the Ion One Touch™ II ES (Thermo Fisher Scientific).
948 Sequencing was performed using the Ion Proton™ System with Ion PI™ Chip kit v3 (Thermo Fisher
949 Scientific). Data was collected using the Torrent Suite ver. 5.0.5 software (Thermo Fisher Scientific).
950 Sequence reads were mapped using Bowtie2 ver. 2.5.4[57] against the assembled genome sequence of
951 Isolate57625. Mapped reads were counted using HTseq ver. 1.99.2[58]. Merged transcript count data were
952 normalized using TCC ver. 1.26.0[76] and differentially expressed genes (DEG) were detected under false
953 discovery rate (FDR) < 0.01.

954

955 ***Phylogenetic tree analysis***
956 The genome sequences of the various clinical isolates shown in Figure S2C for phylogenetic tree analysis
957 were obtained from the NCBI database and are listed in Table S2. Core-genome SNVs were detected using
958 Snippy ver. 4.6.0 (https://github.com/tseemann/snippy) with each assembled genome sequence and the
959 type strain (ATCC 19977, CU458896.1) as the reference. The concatenated core-genome SNVs were also
960 aligned using the snippy-core script. The phylogenetic tree was constructed using IQ-TREE ver.2[60] using
961 the maximum likelihood criterion and rendered using iTOL ver.6.7[61]. Phylogenetic tree analysis of pMAB625
962 sequences was performed by the same method. For the phylogenetic tree analysis regarding the
963 components of the ESX secretion system, the amino acid sequences of ESX loci (*eccB*, *eccC*, *eccD*, *mycP*,
964 and *eccE*) were concatenated and used as input for NGphylogeny.fr[24] using the PhyML+SMS inference
965 method.
966
967 ***PCR for plasmid detection and copy number analysis***
968 PCR was performed using KOD One® PCR Master Mix (TOYOBO) and the primers indicated in Table S1.
969 Amplified DNA was confirmed using agarose gel electrophoresis. The plasmid copy number was analyzed
970 by qPCR using PowerUp™ SYBR™ Green Master Mix (Thermo Fisher Scientific). qPCR was performed
971 using the QuantStudio™ 5 Real-Time PCR System (Thermo Fisher Scientific). Five nanogram of genomic

DNA was used for a 20 µL reaction volume of qPCR. The plasmid copy number is shown as a relative value normalized using the copy number of *HrpA*, which is present in one copy on the chromosome.

Mapping the read data of various clinical isolates to the genome sequence of Isolate57625

Raw read data of *M. abscessus* clinical isolate in Japan, Taiwan[7], China[26], the US, the United Kingdom (UK) and Spain were obtained from the NCBI sequence reads archive (SRA). Raw read data were trimmed using fastp ver. 0.23.4[62] and reduced using seqkit ver.2.4.0[63] to 200 Mb for the Ion Proton™ single-end data and 100 Mb for the Illumina pair-end data to equalize the depth of coverage among isolates. Reads were mapped using BWA-MEM ver. 0.7.17-r1188 against the chromosome and plasmid sequences of Isolate57625 and other plasmids which were hit using PLSDB by the taxonomic searching of "*abscessus*" with removing the redundant plasmid sequences (ANI (%)>97, without large SV (>8 kbp)). The depth of coverage was calculated using Qualimap ver. 2.2.2-dev[77]. The covered genome region was calculated using bedtools ver. 2.30.0[64]. We considered the isolate whose depth of coverage was higher than 10x and the covered genome region was higher than 75% as the plasmid-harboring isolate. The 152 sequences for the analysis of the distribution of plasmids identified in other NTM and previously reported[29] were listed in Table S2. For the phylogenetic tree analysis, the aligned assumed chromosome sequences using Snippy-core script were used as input for Gubbins ver.3.3.1[27]. The phylogenetic tree was rendered using ggtree ver 3.10.1[28].

QUANTIFICATION AND STATISTICAL ANALYSIS

Statistical analysis in this study were performed using R ver. 4.3.1. Statistical significance in Figure S1 were calculated using one-way ANOVA followed by Dunnett's test and data were represents the mean of the three independent experiments and the error bar represents the standard deviation. Statistical analysis of the number of clinical isolates retaining plasmid in Table 4 was performed using Fisher's exact test with Holm's method for correction of multiple comparisons using RVAideMemoire ver. 0.9-83-7 (https://github.com/cran/RVAideMemoire).